Monthly Notices of the ROYAL ASTRONOMICAL SOCIETY

MNRAS **514,** 4828–4844 (2022)
Advance Access publication 2022 June 2

https://doi.org/10.1093/mnras/stac1506

Galaxy pairs in the Sloan Digital Sky Survey – XV. Properties of ionized outflows

William Matzko [1]★ Shobita Satyapal,[1] Sara L. Ellison [2] Remington O. Sexton [1,3] Nathan J. Secrest [3] Gabriela Canalizo,[4] Laura Blecha,[5] David R. Patton [6] and Jillian M. Scudder [7]

[1]*Department of Physics and Astronomy, George Mason University, MS3F3, 4400 University Drive, Fairfax, VA 22030, USA*
[2]*Department of Physics and Astronomy, University of Victoria, Victoria, BC V8P 1A1, Canada*
[3]*U.S. Naval Observatory, 3450 Massachusetts Ave NW, Washington, DC 20392-5420, USA*
[4]*Department of Physics and Astronomy, University of California, Riverside, 900 University Avenue, Riverside, CA 92521, USA*
[5]*Department of Physics, University of Florida, P.O. Box 118440, Gainesville, FL 32611-8440, USA*
[6]*Department of Physics and Astronomy, Trent University, 1600 West Bank Drive, Peterborough, ON K9L 0G2, Canada*
[7]*Department of Physics and Astronomy, Oberlin College, Oberlin, OH 44074, USA*

Accepted 2022 May 26. Received 2022 May 17; in original form 2022 February 10

ABSTRACT

Powerful outflows are thought to play a critical role in galaxy evolution and black hole growth. We present the first large-scale systematic study of ionized outflows in paired galaxies and post-mergers compared to a robust control sample of isolated galaxies. We isolate the impact of the merger environment to determine if outflow properties depend on merger stage. Our sample contains ∼4000 paired galaxies and ∼250 post-mergers in the local universe ($0.02 \leq z \leq 0.2$) from the *Sloan Digital Sky Survey* Data Release 7 (*SDSS* DR 7) matched in stellar mass, redshift, local density of galaxies, and [O III] λ5007 luminosity to a control sample of isolated galaxies. By fitting the [O III] λ5007 line, we find ionized outflows in ∼15 per cent of our entire sample. Outflows are much rarer in star-forming galaxies compared to active galactic nuclei (AGNs), and outflow incidence and velocity increase with [O III] λ5007 luminosity. Outflow incidence is significantly elevated in the optical + mid-infrared selected AGN compared to purely optical AGN; over 60 per cent show outflows at the highest luminosities ($L_{[\mathrm{OIII}]\ \lambda5007} \gtrsim 10^{42}$ erg s^{-1}), suggesting mid-infrared AGN selection favours galaxies with powerful outflows, at least for higher [O III] λ5007 luminosities. However, we find no statistically significant difference in outflow incidence, velocity, and luminosity in mergers compared to isolated galaxies, and there is no dependence on merger stage. Therefore, while interactions are predicted to drive gas inflows and subsequently trigger nuclear star formation and accretion activity, when the power source of the outflow is controlled for, the merging environment has no further impact on the large-scale ionized outflows as traced by [O III] λ5007.

Key words: ISM: jets and outflows – galaxies: active – galaxies: evolution – galaxies: interactions.

1 INTRODUCTION

Hierarchical models of the Universe and observations suggest that mergers play a critical role in galaxy evolution. Mergers are thought to drive morphological transformations (e.g. Toomre & Toomre 1972; Schweizer 1982; Rothberg & Joseph 2004), trigger star formation (e.g. Ellison et al. 2008; Woods et al. 2010; Patton et al. 2011, 2013; Wong et al. 2011; Liu, Shen & Strauss 2012; Scudder et al. 2012b), and trigger AGN (e.g. Canalizo & Stockton 2001; Hopkins et al. 2008; Ellison et al. 2011; Lackner et al. 2014; Satyapal et al. 2014; Weston et al. 2017; Blecha et al. 2018; Goulding et al. 2018), although the merger-AGN connection is a topic of vigorous debate, particularly at higher redshifts (Cisternas et al. 2011; Kocevski et al. 2012; Simmons et al. 2012; Villforth et al. 2014, 2017; Rosario et al. 2015; Schawinski et al. 2015; Bruce et al. 2016; Mechtley et al. 2016; Shah et al. 2020). Similarly, the connection between mergers and star formation at higher redshifts is also debated (Khochfar & Silk 2011; Xu et al. 2012; Kaviraj et al. 2013; Perret et al. 2014; Fensch et al. 2017; Pearson et al. 2019). Despite these debates, the currently accepted paradigm of galaxy evolution begins with young, blue disc galaxies merging and ends with the formation of large 'red and dead' elliptical galaxies, where some form of feedback from the enhanced nuclear activity is required to quench star formation in the host galaxies.

An outflow is one form of feedback that is typically invoked as the primary mechanism that suppresses star formation in such mergers. However, it is not completely clear if these outflows are sufficient to cause quenching (e.g. Springel, Di Matteo & Hernquist 2005; Hopkins et al. 2006; Pereira-Santaella et al. 2018; Fluetsch et al. 2019; Ellison et al. 2021), or if they result in an elevation in the star formation activity (e.g. Silk 2013; Zubovas et al. 2013; Cresci et al. 2015). None the less, outflows have long been known to be present in purely star forming, isolated galaxies at low redshifts (e.g. Heckman, Armus & Miley 1990; Rupke, Veilleux & Sanders 2005a) and more moderate ($0.5 \lesssim z \lesssim 1$) redshifts (e.g. Nestor et al. 2011; Geach et al. 2018). For recent reviews, see Rupke (2018) and Veilleux et al. (2020). In star-forming galaxies, there are clear indications

★ E-mail: wmatzko@gmu.edu

that the incidence and velocity of the outflows are correlated with the stellar mass, central concentration, star formation rate, and star formation surface density, with a clear increase in the incidence in the most active star-forming galaxies (e.g. Rupke, Veilleux & Sanders 2005b; Davies et al. 2019; Leung et al. 2019), with the latter two examining high-redshift samples ($1 \lesssim z \lesssim 4$). Indeed, powerful outflows are found to be ubiquitous in high-redshift star-forming galaxies, where the star formation rates and surface densities are high (Weiner et al. 2009; Rubin et al. 2010; Genzel et al. 2011; Förster Schreiber et al. 2019; Swinbank et al. 2019). Outflows have also long been known to be present in isolated AGN, with clear indications that their incidence and velocities are correlated with AGN luminosity and perhaps Eddington ratio (e.g. Woo et al. 2016; Lutz et al. 2020; Wylezalek et al. 2020; Avery et al. 2021). Radio properties (e.g. radio luminosity) of galaxies can also play a role in outflow incidence and properties (e.g. Zakamska & Greene 2014; Molyneux, Harrison & Jarvis 2019; Santoro et al. 2020); however, we do not explore the radio properties of the galaxies in our sample in this work.

It is well-known that nuclear star formation and accretion activity are both enhanced in mergers and show a clear dependence on merger stage (e.g. Ellison et al. 2011, 2013b; Satyapal et al. 2014). It is thus expected that outflows would be prevalent in mergers, and that their incidence and properties might show a dependence on merger stage. Indeed, many studies have detected outflows in interacting galaxies and mergers (e.g. Rupke et al. 2005a; Rupke, Veilleux & Sanders 2005c; Soto & Martin 2012; Westmoquette et al. 2012; Veilleux et al. 2013; Baron et al. 2018; Geach et al. 2018; Pereira-Santaella et al. 2018; Herrera-Camus et al. 2020; Guolo-Pereira et al. 2021). However, these studies have by and large been carried out on small samples of galaxies, and often target 'extreme' objects, such as ultraluminous infrared galaxies (ULIRGs) or dust reddened quasars (e.g. Sturm et al. 2011; Cicone et al. 2014; Rupke, Gültekin & Veilleux 2017; Lutz et al. 2020; Veilleux et al. 2020; Fluetsch et al. 2021, and references therein), which are not representative of the general galaxy population. In addition to these studies, follow-up observations of the several hundred galaxies with double-peaked narrow emission line profiles in optical surveys have revealed that the vast majority are associated with gas outflows in mergers (e.g. Barrows et al. 2013; Müller-Sánchez et al. 2015; Comerford et al. 2018; Nevin et al. 2018) in both low and moderate ($z \lesssim 1.6$) redshifts, again suggesting a close tie between galaxy–galaxy interactions and the presence of outflows. There have also been attempts to quantify the relative role played by star formation and accretion activity on driving the outflows, with indications that the outflow incidence and velocities are higher in galaxies harbouring AGN (e.g. Harrison et al. 2016; Concas et al. 2017; Smethurst et al. 2019; Avery et al. 2021), even at redshifts out to $z \sim 3.8$ (Leung et al. 2019).

While it is clear that outflows are associated with galaxy mergers, it is unclear how the merger environment itself impacts the incidence and properties of these outflows. In order to determine the effect of the merger on the outflows, a systematic study of outflows in mergers compared to a matched control sample of isolated galaxies must be conducted. However, there has thus far been no large-scale systematic study that examines the properties of outflows in galaxy mergers compared with isolated galaxies to determine if the merger environment enhances or suppresses the outflowing material, and to explore how the presence and properties of outflows depend on merger stage. Most importantly, since there have not yet been any outflow studies in which galaxy mergers have been compared to a matched control sample of isolated galaxies, the exact effect of mergers on outflows is not yet known, and the dependence of outflow properties on merger stage is completely unexplored. Since mergers induce gas inflows (e.g. Barnes & Hernquist 1991; Blumenthal & Barnes 2018), it might be natural to expect that the outflow incidence and properties are suppressed in merging galaxies compared to isolated galaxies. Alternatively, the gas inflows and subsequent increase in the central gas densities might cause the outflows to sweep up more material, thereby increasing the outflow luminosity and resulting in an enhancement of the outflow incidence and energetics in mergers. Mergers also cause a dilution of the central gas phase metallicity (e.g. Kewley et al. 2010; Ellison et al. 2013b; Thorp et al. 2019). Together with the enhanced nuclear activity, mergers may disturb the interstellar medium (ISM) in some way that enhances the outflows. Given that galaxy mergers are thought to play a major role in a galaxy's morphology, star formation rate, nuclear accretion rate, metallicity, and gas content, exploring the incidence and properties of outflowing gas in mergers is of fundamental importance to our understanding of the critical role galaxy mergers play in galaxy evolution.

In this paper, we carry out the first large-scale systematic study of outflows in merging environments compared to non-merging environments. This paper builds upon a large body of work on galaxy pairs and post-mergers, drawn from the *Sloan Digital Sky Survey* (*SDSS*), that uses robust control samples of isolated galaxies to quantify the impact of mergers on galaxy and AGN properties (Ellison et al. 2008, 2010, 2011, 2013a,b; Patton et al. 2011, 2013, 2016; Scudder et al. 2012b, 2015; Satyapal et al. 2014; Ellison, Patton & Hickox 2015). Here, we utilize the [O III] λ5007 emission line to trace ionized gas in pairs, post-mergers, and isolated galaxies, with the goal of isolating the impact of the merging environment on outflow properties. We examine ∼4000 paired galaxies and ∼250 post-mergers, consisting of AGN and star-forming (SF) galaxies, matched to a control sample of ∼12 000 galaxies. In Section 2, we provide details on the construction of the pair, post-merger and control samples, and discuss our fitting procedure and outflow selection criteria in Section 3. In Section 4, we discuss the bulk outflow characteristics of our sample, while in Section 5 we examine outflow properties as a function of projected physical separation (r_p). In Section 6, we discuss the implications of our results, and Section 7 contains a results summary and directions of future work. Throughout this paper, we assume a flat Lambda cold dark matter (ΛCDM) cosmology with $H_0 = 70$ km s^{-1} Mpc^{-1}, $\Omega_m = 0.27$, and $\Omega_\Lambda = 0.73$.

2 SAMPLE SELECTION

2.1 Galaxy pair and post-merger samples

The galaxy-merger sample used in this work has been described in depth in previous papers in this series and is drawn specifically from the sample described in Satyapal et al. (2014). We refer the reader to this previous work for full details on the sample, and the careful considerations applied to remove any selection effects. In brief, the pairs sample consists of close spectroscopic galaxy pairs, and visually classified post-mergers from the *Sloan Digital Sky Survey Data Release* 7 (*SDSS DR*7, Abazajian et al. 2009) Main Galaxy Sample. The extinction-corrected *r*-band Petrosian magnitudes are between $14.0 \leq m_r \leq 17.77$, the redshift range is $0.02 \leq z \leq 0.2$, and all objects are spectroscopically classified as a galaxy. Projected physical separations are required to be $r_p \leq 80 h_{70}^{-1}$ kpc and the relative velocity must be $\Delta V \leq 300$ km s^{-1}. Further, the stellar mass ratios between the pairs must be $0.25 \leq M_1/M_2 \leq 4$ in order to select major mergers. It should be noted that not every galaxy

pair is visibly interacting; it is possible some of these galaxies may never merge or are non-interacting projected pairs. These galaxies are referred to as 'paired galaxies'.

The visually classified post-merger sample is initially drawn from the Galaxy Zoo (Lintott et al. 2008) catalogue presented by Darg et al. (2010). Ellison et al. (2013b) imposed further restrictions on the post-merger sample by removing 'normal' irregular galaxies and pairs that have not fully coalesced into an appropriate post-merger state, among other requirements. This sample of visually classified post-merger galaxies is referred to as the post-merger sample.

For convenience, we will refer to the paired galaxies, which represent the 'early' stages of galaxy interactions (0–80 kpc), and the post-merger sample, which represents the 'late' stages of galaxy interactions (i.e. post-coalescence), collectively as the 'merger' sample.

Finally, the merger sample is matched to the final public all-sky *Wide-field Infrared Survey Explorer* (*WISE*) source catalogue,[1] where a merger is matched if the positions agree to within six arcsec. Since we employ mid-infrared AGN classification in one of our sub-samples (as discussed in the paragraph below), we require that all objects be detected with a signal-to-noise greater than 5σ in the 3.4 μm *W*1 and 4.6 μm *W*2 bands. Our initial merger sample thus consists of 321 post-mergers and 5026 paired galaxies, with $\sim$ 55 per cent of galaxies meeting the *WISE* detection criteria.

The galaxies in our sample are classified as AGN or SF galaxies based on optical narrow emission line ratio Baldwin–Phillips–Terlevich (BPT) diagnostics (Baldwin, Phillips & Terlevich 1981) and mid-infrared colour selection. For optical selection, we use the traditional K03 (Kauffmann et al. 2003) and K01 (Kewley et al. 2001) selection criteria to classify galaxies as K01 AGN, K03 AGN, and K03 SF using extinction-corrected fluxes provided by Scudder, Ellison & Mendel (2012a). K01 AGN are taken to be 'pure' AGN, whereas K03 AGN are dominated by AGN activity, but starbursts may contribute to the ionized emission. K03 SF galaxies (hereafter SF galaxies) are dominated by stellar activity, but may have a small contribution (up to 3 per cent, Stasińska et al. 2006) from AGN. However, see Agostino et al. (2021) for an alternative view on the 'mixing sequence' picture. We remove possible AGN contamination from our SF sample by requiring our SF galaxies to have a *WISE* colour cut of $W1 - W2 < 0.5$ since optical flags might not detect some AGN, especially in late-stage mergers when AGNs are highly obscured by gas and dust (Satyapal et al. 2014; Ellison et al. 2019). Since mid-infrared selected AGNs are more common in mergers (Satyapal et al. 2014; Blecha et al. 2018), we also sub-divide the merger sample into '*WISE* + BPT' AGN to determine if mid-infrared selection has an impact on outflow properties. Here, we require both an optical AGN (either K01 or K03) and an infrared AGN detection ($W1 - W2 > 0.5$). While the *WISE* colour cut we impose here is more relaxed than the common $W1 - W2 > 0.8$ cut, it is not significantly less reliable and provides a more complete sample of AGN at $z \lesssim 0.5$ (Blecha et al. 2018). We require the *WISE* AGN to be BPT AGN so we can control for the power source of the outflow; since we impose an [O III] λ5007 luminosity matching requirement between mergers and controls (see below paragraph), we want to ensure the [O III] λ5007 is tracing the AGN luminosity. Galaxy properties such as the stellar mass and total star formation rate (SFR) are taken from the Mendel et al. (2014) and Brinchmann et al. (2004) catalogues. We note that while the SFR for SF galaxies is computed by modelling the Hα emission line, the SFR for AGN is computed using D4000.

[1] https://wise2.ipac.caltech.edu/docs/release/allsky/

2.2 Matched control sample

The merger sample is compared to a set of physically similar isolated galaxies, drawn from the same data base as the mergers, so that each merger has a matched set of controls associated with them. We consider a galaxy to be isolated if the projected distance r_p to its closest spectroscopic companion is greater than 200 kpc. As discussed in Perez, Tissera & Blaizot (2009) and following Ellison et al. (2010, 2013a) and Scudder et al. (2012b) controls are matched simultaneously in redshift, mass, and local density of galaxies, all of which may show a dependence on outflow incidence and properties. Since the [O III] λ5007 luminosity can affect outflow properties (see Fiore et al. 2017), we also match in this parameter. Further, matching in redshift and [O III] λ5007 luminosity ensures that our ability to detect an outflow will not be biased towards either the mergers or controls. SF galaxies are additionally matched in SFR. The local density of galaxies is defined as

$$\Sigma_n = \frac{n}{\pi d_n^2}, \tag{1}$$

where d_n is the projected distance in Mpc to the nth nearest neighbour within ± 1000 km s^{-1}. Normalized densities δ_n are computed relative to the median Σ_n within a redshift slice of ± 0.01. Following Satyapal et al. (2014), we take $n = 5$. Intuitively, this local density of galaxies describes the large-scale neighbourhood of a given galaxy. In our case, we use the fifth nearest neighbour to characterize this density. As explained in Perez et al. (2009) and Ellison et al. (2010), this parameter is sensitive to the SFR and gas content of a galaxy – isolated galaxies can have larger amounts of cold gas and subsequently enhanced star formation compared to mergers. Hence, an unbiased control sample must account for this parameter.

The matching tolerance on redshift is ± 0.05, while for mass and local galaxy density it is ± 0.1 dex. The [O III] λ5007 luminosity tolerance is ± 10 per cent. We attempt to match each object in our merger sample with three *unique* controls. Mergers that could not be matched with at least three unique controls were dropped from the sample. Our matching criteria leaves us with 1906 SF mergers, 1375 K03 AGN mergers, 562 K01 AGN mergers, and 72 WISE + BPT AGN mergers, including paired galaxies and post-mergers.

We note that while we do employ *WISE* colour cuts on our control sample when appropriate (e.g. when making the control sample for *WISE* + BPT AGN and filtering AGN from our SF control sample), the *WISE* controls do not necessarily have the same 5σ detection in the first three *WISE* bands as the mergers do.

3 SPECTRAL FITTING PROCEDURES AND OUTFLOW CRITERIA

3.1 Spectral fitting software

We use the [O III] λ5007 emission line to trace outflows in all mergers and controls. This line is one of the strongest features in the optical spectrum of all emission line galaxies, and is located in a wavelength region free from strong stellar absorption features. Since it is produced in the lower density narrow line region, any asymmetry and broadening of the profile can often be attributed to large-scale winds. For these reasons, it is commonly used in the literature to search for and characterize outflows (e.g. Harrison et al. 2014; Bae & Woo 2016; Cicone, Maiolino & Marconi 2016; Kakkad et al. 2016; Zakamska et al. 2016; Wylezalek et al. 2020). Spectral fitting is done with the open-source PYTHON code Bayesian AGN Decomposition Analysis for *SDSS* Spectra (BADASS) version

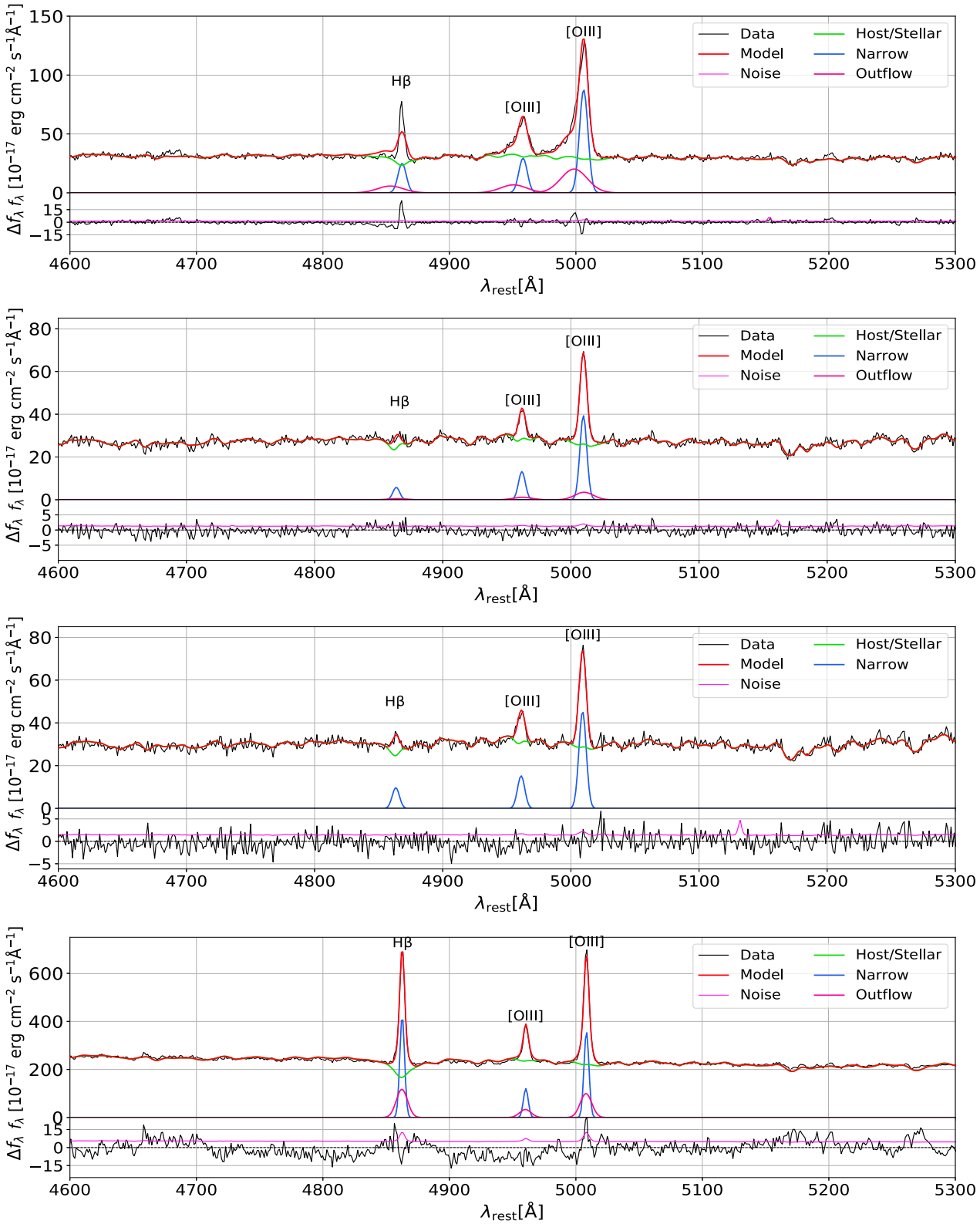

Figure 1. Example spectra fits. Subsequent identifiers are the DR7 SpecObjIDs. *Top panel*: AGN SDSS 456217686624436224 exhibits a reasonably strong outflow detected both in the initial testing and with EMCEE. The bad fit to the H β emission line is caused by a poor stellar template match to the continuum and does not impact our results. *Second to top panel*: AGN SDSS 407803917544456192 was fit for an outflow with EMCEE, but the fit was not significant enough to be classified as an outflow. *Second to bottom panel*: AGN SDSS 160665218618228736 failed the initial testing, hence EMCEE did not fit it for an outflow. *Bottom Panel*: SDSS 631860897941291008 shows a reasonably strong outflow in a SF galaxy.

Table 1. Bulk properties of each sub-sample. The average for each sub-sample property along with upper and lower errors are given. Outflow fraction errors were computed using binomial statistics with a 95 per cent confidence interval. A 2σ mean standard error is used for all other errors. Note that the outflow luminosity listed here refers to the luminosity in the outflow component of the line profile, and we only require mergers to have one successfully analysed control.

Property	K03 SF Merger	K03 SF Control	K01 AGN Merger	K01 AGN Control	K03 AGN Merger	K03 AGN Control	*WISE* + BPT Merger	*WISE* + BPT Control
Total objects	1906	5396	562	1610	1375	3922	72	205
$\log_{10}(L_{[O\,III]\,\lambda5007})$ (erg s^{-1})	$40.44^{0.03}_{0.03}$	$40.44^{0.2}_{0.2}$	$41.09^{0.09}_{0.09}$	$41.09^{0.05}_{0.05}$	$40.91^{0.06}_{0.06}$	$40.90^{0.03}_{0.03}$	$41.63^{0.13}_{0.13}$	$41.63^{0.08}_{0.08}$
Outflow fraction (per cent)	$0.52^{0.44}_{0.27}$	$0.56^{0.24}_{0.18}$	$14.06^{3.20}_{2.80}$	$14.47^{1.81}_{1.68}$	$7.34^{1.51}_{1.32}$	$7.73^{0.88}_{0.82}$	$38.89^{12.22}_{11.27}$	$42.44^{7.10}_{6.90}$
$\log_{10}(L_{outflow})$ (erg s^{-1})	$40.06^{0.31}_{0.31}$	$40.03^{0.18}_{0.18}$	$40.71^{0.13}_{0.13}$	$40.72^{0.07}_{0.07}$	$40.66^{0.12}_{0.12}$	$40.69^{0.06}_{0.06}$	$40.80^{0.18}_{0.18}$	$40.87^{0.09}_{0.09}$
Outflow velocity (km s^{-1})	400^{250}_{250}	320^{80}_{80}	690^{70}_{70}	730^{40}_{40}	700^{70}_{70}	720^{30}_{30}	710^{140}_{140}	830^{80}_{80}
$\log_{10}$(SFR) ($M_\star$ yr^{-1})	$0.54^{0.02}_{0.02}$	$0.53^{0.01}_{0.01}$	$0.44^{0.28}_{0.28}$	$0.15^{0.04}_{0.04}$	$0.52^{0.10}_{0.10}$	$0.44^{0.02}_{0.02}$	$0.94^{0.17}_{0.17}$	$0.81^{0.09}_{0.09}$

7.6.5.[2] A full description of the code can be found in Sexton et al. (2021). Here, we just give a brief summary of the fitting techniques and input parameters. BADASS works by modelling various spectral components (e.g. power-law continuum, emission lines, etc.) and sequentially subtracting them from the spectra to be fit independently. Once these components are subtracted off, only the underlying stellar continuum remains. The stellar continuum may be fit with either empirical stellar templates or a single stellar population model, depending on the quality (signal-to-noise ratio, S/N) of the spectrum. Emission lines may be fit with a variety of line profiles, but here we use a Gaussian profile that is fit for amplitude, FWHM, and velocity offset. Initial fits to the spectra are obtained using the SLSQP algorithm from the standard PYTHON library SCIPY.OPTIMIZE.MINIMIZE. The parameter fits from this algorithm are then used as the initial guesses for a Markov Chain Monte Carlo (MCMC) algorithm, implemented by the EMCEE package (Foreman-Mackey et al. 2013), to estimate robust parameter uncertainties.

Outflow presence may be (and, in this work, is) tested for during the initial fit by fitting both a single Gaussian and a double Gaussian model to the [O III] λ5007 emission line. The fit is repeated for a set number of iterations (50 in our case) with slightly different initial guesses, which provides a more reliable estimation of parameter values than a single fit. The median value for the fitted parameters is used to assess the possible presence of outflows by comparing the fitted parameters (amplitude, FWHM, and velocity offset) of the 'core' and outflowing line components. If the uncertainty overlap between the core and outflowing component for one of these parameters is within a certain user-defined σ value (e.g. $1\sigma, 2\sigma$), then BADASS assumes there is no outflow. In addition to this uncertainty check, a statistical F-test is performed to compare the single and double Gaussian models. This test effectively calculates how much better the double Gaussian fit is and if using it is justified. The resulting F-statistic is converted to a p-value, and if it is less than a user-defined value then BADASS assumes there is no outflow. If the preliminary outflow tests are passed, the final fit using EMCEE will include an outflow component in the model.

The AGNs we are fitting are type II AGN, so we disable unnecessary fitting components (namely AGN power law, broad lines, and Fe II contamination). For the preliminary outflow testing, we check for overlapping uncertainties in the FWHM and velocity offset parameters, and apply the F-test as described above. Although the purpose of the preliminary outflow testing is to discard spectra that clearly do not have outflows, there is a danger that a weak outflow will be overlooked during the initial fit. To guard against that, we apply generous cutoffs for the outflow tests. Specifically, we only require the core component and outflow component FWHM and velocity offset parameters to be different at a 0.5σ level, and the F-test p-value be greater than 0.70. Fits with outflows that do not meet the initial criteria for detection will not significantly improve in the final fit using MCMC, and will hence not be reliably detected. False-positives detected by EMCEE will be flagged when the final fits are analysed (see Section 3.2). The SF spectra are fit in the same way as the AGN spectra. However, we do not require outflows to be blueshifted in the SF galaxies because outflows in SF galaxies have a much more symmetrical line profile even in the presence of outflows and are thus much harder to detect (see Sections 3.2 and 4).

For both the AGN and SF spectra, we run the MCMC sampler for a minimum of 5000 iterations and a maximum of 25 000 iterations using 20 walkers. We use the 'median' convergence option in the autocorrelation analysis which uses the median autocorrelation time of all free parameters to assess if the MCMC chains have converged. Effectively, if enough parameters have converged, the MCMC analysis will stop before it reaches 25 000 iterations. Once the parameters have converged, the MCMC will continue sampling for 5000 iterations. These iterations are used to generate the posterior distribution and subsequently the best-fitting parameter values and their uncertainties.

It should be noted that BADASS will not fit spectra that are of insufficient quality, as determined by the number of 'good' channels. A good channel is defined by having flux and flux errors greater than zero at each pixel, and not being flagged by the *SDSS* for having bad pixels. If the fraction of good channels in a spectrum is less than 60 per cent, then the spectrum will not be fit. This will cause additional mergers to be dropped from the final analysis, since a merger that was matched with three controls may not have three controls that are of sufficient quality.

3.2 Outflow selection criteria

As discussed in Section 3.1, we use a SLSQP bootstrap algorithm to perform an initial test for outflows, as well as a statistical F-test. For this initial test, we require that the outflowing component be broader than the core by only 0.5σ. Further, the p-value returned by the F-test must be greater than 0.70, indicating we are 70 per cent confident that our [OIII] λ5007 line profile is best modelled by two Gaussian components instead of one. If a spectrum passes the initial outflow

[2] https://github.com/remingtonsexton/BADASS3

test, then an outflow component is included in the final MCMC model. Even if BADASS detects an outflow in the initial fit, the final fit given by EMCEE may not be reliable. To ensure outflows are robustly detected, the final fits must meet the following criteria. First, the outflow amplitude must be at least 1σ above the noise floor of the spectrum. Secondly, the FWHM of the outflow component must be larger than the FWHM of the 'core' line within 1σ (in other words, the FWHM values between the line core and outflow component should not overlap within the uncertainties given by MCMC). Finally, for AGN only, the velocity offset of the outflow component must be blueshifted with respect to the core line by at least 1σ. This blueshift requirement is consistent with numerous other studies that interpret broad, blue-wing components of emission lines as outflow signatures (e.g. Holt, Tadhunter & Morganti 2008; Mullaney et al. 2013; Zakamska & Greene 2014; Carniani et al. 2015; Balmaverde et al. 2016; Harrison et al. 2016; Kakkad et al. 2016; Geach et al. 2018; Guolo-Pereira et al. 2021). Note that we do not impose a blue-shift requirement on the outflow component for SF galaxies. The vast majority of [O III] λ5007 line profiles in SF galaxies are highly symmetrical, but some show an underlying broad component or a slightly blue-shifted asymmetry in their line profile. We choose to be inclusive in our outflow definition for SF galaxies such that the profiles with an underlying broad component are flagged as outflows. The physical motivation for this decision is presented in Kadir et al. (in preparation), where they employ the biconical outflow model of Bae & Woo (2016) and simulate the effects of extinction on the outflowing [O III] λ5007 line profile in an obscuring medium. These simulations show that when outflows arise from extended regions, as expected in SF galaxies, the observed line profile arising from the *integrated* emission from the outflow is less affected by extinction and therefore displays a more symmetrical line profile compared to an outflow arising from a compact region of deeply embedded gas around an AGN. While we choose to relax the blue-shift requirement for SF galaxies for these reasons, we point out that the outflow incidence in SF galaxies is not significantly altered if the blue-shift requirement is imposed – the outflow incidence decreases from $\sim$0.5 to $\sim$0.4 per cent in both the merger and control samples – leaving the results from this work unchanged. Similarly, if we relax the blue-shift requirement in our AGN to account for more uncommon outflow line profiles, such as redshifted profiles or underlying broad profiles, the number of outflows in our AGN merger and control samples increases by 280. However, this increase does not alter our conclusions. We finally visually inspect the final fits and discard 11 lingering spurious outflow detections in the entire sample of mergers and controls.

Of course, our ability to detect an outflow will depend on the S/N of the spectrum. The majority (>90 per cent) of spectra in our sample have a S/N greater than five in the [O III] λ5007 line, with only about two per cent of the sample having a S/N less than three. Although we have no explicit S/N requirement when matching the mergers to controls, by matching in [O III] λ5007 luminosity and redshift we ensure that our ability to detect an outflow is not biased towards either the merger or its associated controls (assuming the aperture and exposure time is the same, or nearly so, for all targets).

It should be noted that there is no single definition of an outflow when examining emission lines. While blue-shifted absorption lines provide an unambiguous signature of outflows (Veilleux et al. 2013), the exact origin of the broad, blue-shifted, component of emission lines is more uncertain. As discussed in Cicone et al. (2016), such a component may be the result of galaxy interactions or virialised motions within the galaxy. Further, outflows can produce a variety of emission line profiles; depending on outflow orientation and dust extinction, an outflow might create a non-Gaussian or redshifted Gaussian line profile (Bae & Woo 2016). Outflows may also create a double-peaked [O III] λ5007 emission line profile (e.g. Comerford et al. 2018; Nevin et al. 2018). Dual AGN may also generate a double-peaked line profile (e.g. Rosario et al. 2011), but high resolution imaging and spectroscopy suggest that the majority of these double-peaked line profiles are associated with outflows (e.g. Shen et al. 2011; Müller-Sánchez et al. 2015). Regardless, our outflow selection criteria, as explained earlier in Section 3.2, is well-justified by the literature.

Similarly, there is no single definition of outflow velocity. A common measure of outflow velocity is W_{80} (e.g. Zakamska & Greene 2014), which is defined as the flux enclosing 80 per cent of the emission line. For a Gaussian profile, there is a simple relation between W_{80} and the FWHM of the line, namely $W_{80} = 1.088$ FWHM. However, there are other common measures of outflow velocity, the main difference being the velocity offset $v_{\rm off}$ between the outflow and core emission line component is taken into account. While this definition is also used (e.g. Toba et al. 2017; Manzano-King, Canalizo & Sales 2019), we prefer to use the W_{80} metric because $v_{\rm off}$ is sensitive to the amount of extinction in a galaxy (Bae & Woo 2016), and our mergers have a higher amount of extinction than our controls (see Section 6).

Fig. 1 shows example fits to a variety of spectra. Various cases corresponding to different outflow test conditions described above are highlighted, including a strong outflow detection in an AGN, an outflow that was 'found' during preliminary testing but was not significant when fit with EMCEE, no outflow detection at all, and an outflow detection in an SF galaxy. We note that the outflow in the AGNs are much more asymmetrical than it is in the SF galaxy. Indeed, this is a general characteristic with outflows in our sample – SF galaxies, even in the presence of outflows, are much more symmetrical than their AGN counterparts (again, see Section 4).

4 GENERAL OUTFLOW CHARACTERISTICS IN THE SAMPLE

Since our sample allows us to explore the dependence of outflow incidence and properties with various galaxy properties in a large, statistically significant sample, we first present the general results from our analysis in our full sample. In Table 1, we show selected properties of the full merger and control samples for each of the sub-classes. Quoted values are the average of the entire sub-sample that could be matched with three unique controls, at least one of which was successfully fitted by BADASS. Uncertainties on the outflow incidence fraction are given by binomial counting statistics with a two-sided 95 per cent confidence interval, in accordance with Gehrels (1986). All other uncertainties in the table are given by the standard error of the mean, multiplied by 1.96 for the 95 per cent confidence interval.

From Table 1, we observe several clear results on the general characteristics of the sample. First, the fraction of SF galaxies (both mergers and controls) with outflows is significantly lower (between a factor of $\sim$14 for K03 AGN and a factor of $\sim$80 for *WISE* + BPT AGN) compared to all of the AGN sub-samples. This is also clearly seen in Fig. 2, where it is readily apparent that the outflow fraction is much higher in the AGN-dominated region of the BPT diagram. This is in qualitative agreement with a number of other studies that reveal that the outflow incidence is significantly lower in SF galaxies compared to AGNs (e.g. Cicone et al. 2016;

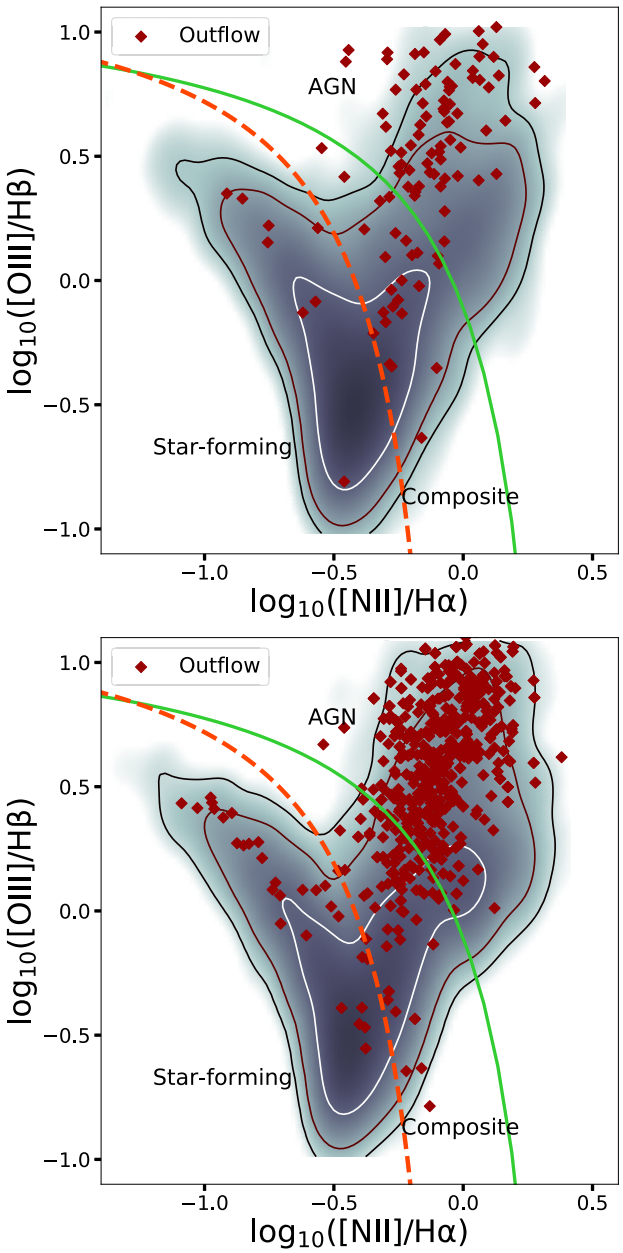

Figure 2. BPT diagrams of the entire merger (top panel) and control (bottom panel) samples. Darker colours indicate denser regions populated by objects with no outflows. Contours enclose the regions containing 99.5, 95, and 68 per cent of the objects without outflows. The orange dashed line denotes the K03 SF curve, below which galaxies are dominated by star formation. The solid green line denotes the K01 AGN curve, above which galaxies are dominated by AGN. Red diamonds indicate objects with outflows.

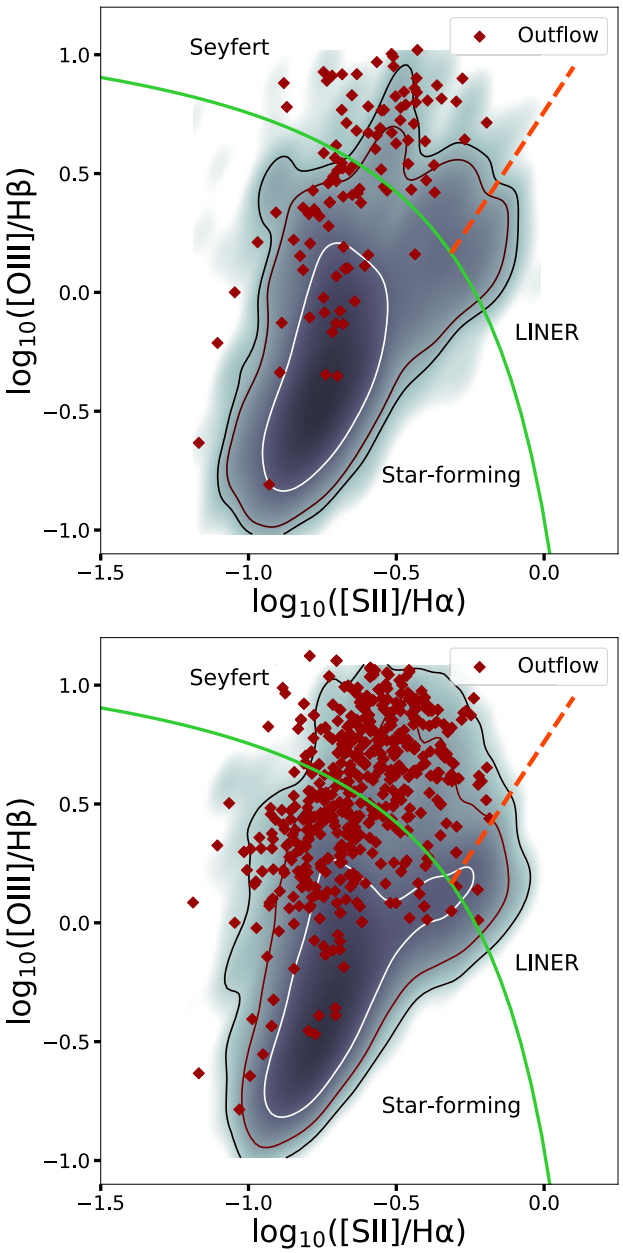

Figure 3. Alternate BPT diagram of the entire merger (top panel) and control (bottom panel) samples. Darker colours indicate denser regions populated by objects with no outflows. Contours enclose the regions containing 99.5, 95, and 68 per cent of the objects without outflows. The solid green line separates AGN from SF galaxies, while the orange dashed line separates Seyfert galaxies from LINERs. Red diamonds indicate objects with outflows.

Concas et al. 2017; Manzano-King et al. 2019). Further, Figs 3 and 4 show alternate BPT diagrams, both of which indicate outflows are not common in low-ionization nuclear emission-line regions (LINERs). This is in contrast to what was found by Hermosa Muñoz et al. (2022), where they detected ionized outflows in ∼50 per cent of their LINER sample. However, even though our sample luminosities are comparable, their observations make use of higher resolution IFU data which is generally more sensitive to outflow detections than our lower resolution data (see Section 6).

From Table 1, we also see that the outflow fraction in optical + mid-infrared selected AGNs is roughly a factor of four times higher than the outflow fraction in optically selected AGNs, and almost two orders of magnitude higher than that found in SF galaxies. This is also clearly seen in Fig. 5, which shows the *WISE* colour–colour diagram for our full sample.

We further note that there is no statistically significant difference between the mergers and controls in any of our four samples (SF, K03 AGN, K01 AGN, and *WISE* + BPT AGN) in Table 1. However,

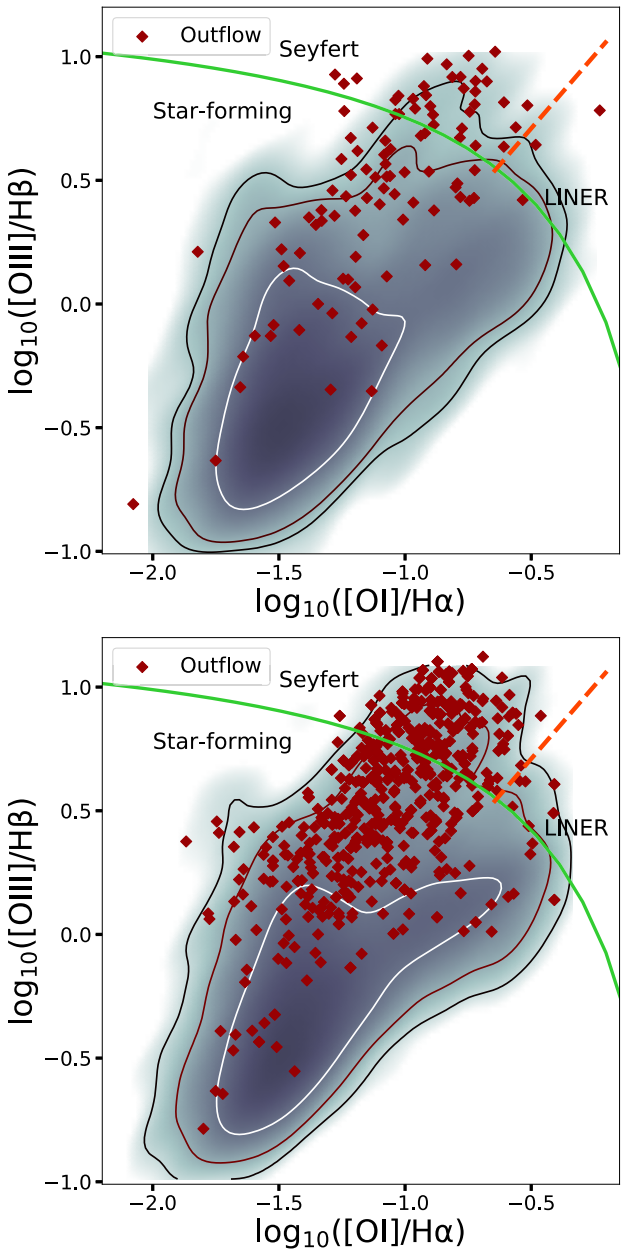

Figure 4. Alternate BPT diagram of the entire merger (top panel) and control (bottom panel) samples. Darker colours indicate denser regions populated by objects with no outflows. Contours enclose the regions containing 99.5, 95, and 68 per cent of the objects without outflows. The solid green line separates AGN from SF galaxies, while the orange dashed line separates Seyfert galaxies from LINERs. Red diamonds indicate objects with outflows.

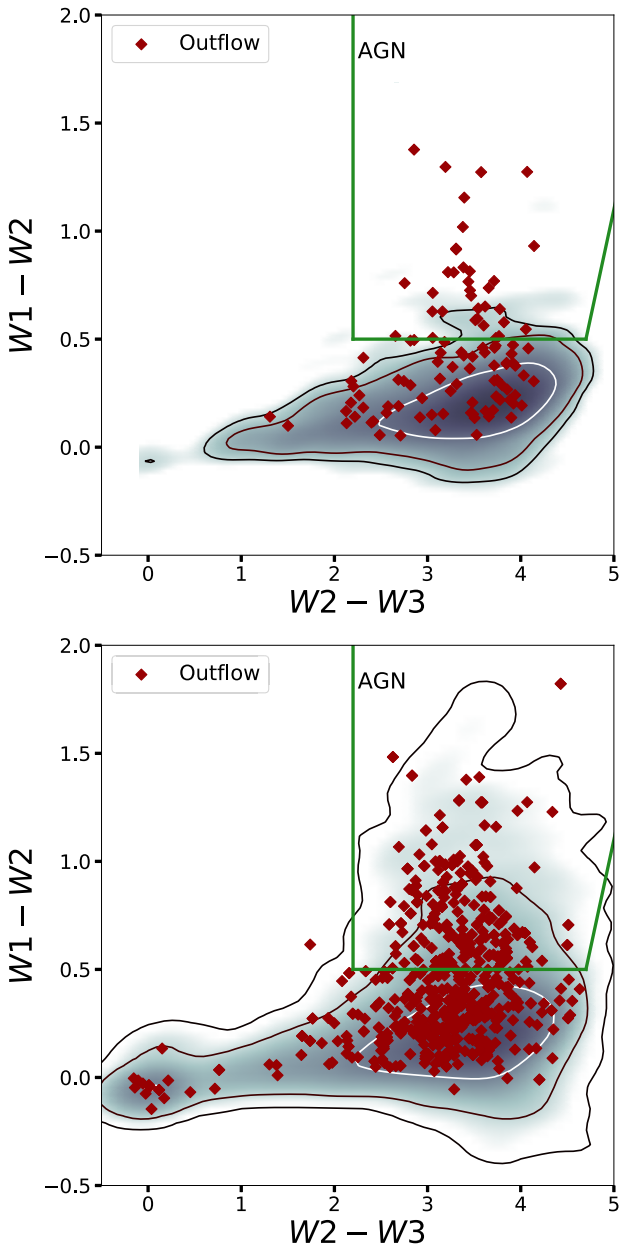

Figure 5. *WISE* colour–colour diagrams of the entire merger (top panel) and control (bottom panel) sample. The green box displays the mid-infrared colour cut described in Blecha et al. (2018), with *WISE* AGN populating the box's interior. Note our colour cut only requires $W1 - W2 > 0.5$. Red diamonds indicate objects with outflows. Darker colours indicate denser regions populated by objects with no outflows. Contours enclose the regions containing 99.5, 95, and 68 per cent of the objects without outflows.

the four samples do show a statistically significant difference in their outflow incidence, with the more stringent AGN selection techniques displaying higher outflow incidences. Indeed, only ∼0.5 per cent of the SF galaxies have an ionized outflow. K03 AGNs have a much higher outflow incidence near ∼7.5 per cent, while K01 AGNs have an outflow incidence of ∼14 per cent. The *WISE* + BPT AGNs have the largest outflow incidence by far at ∼40 per cent.

At first glance, the excess of outflows in optical + mid-infrared selected AGN might simply seem to be a consequence of the variation in the luminosity across the sub-samples, with mid-infrared selected AGNs representing the more luminous objects in the sample. Intuitively, more luminous galaxies can, in principle, drive more luminous outflows which are easier to detect, a result that is indeed reported in a number of previous works (Hill & Zakamska 2014; Woo et al. 2016; Concas et al. 2017; Avery et al. 2021). The trend of outflow incidence increasing with [O III] λ5007 luminosity is also seen in the general properties of our samples, as shown in Fig. 6. Here, objects with outflows are noticeably skewed towards higher [O III] λ5007 luminosity values. However, the increased outflow incidence in optical + mid-infrared selected AGN is not simply a consequence of variation in [O III] λ5007 luminosity across the

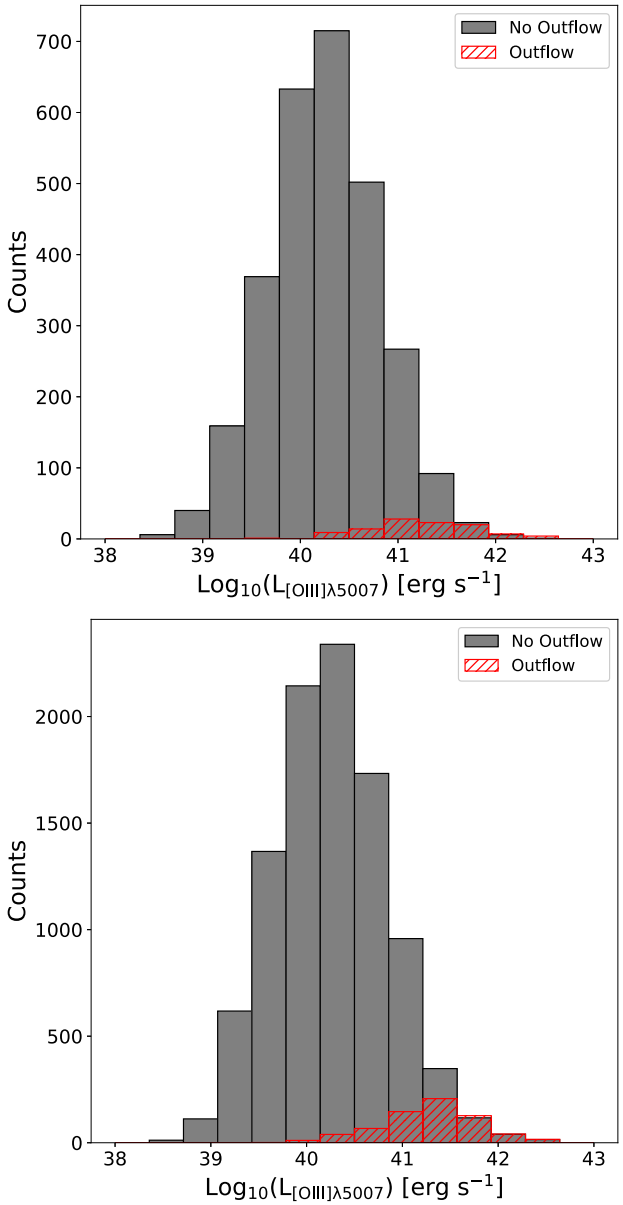

Figure 6. Distribution of [O III] λ5007 luminosity of the entire merger (top panel) and control (bottom panel) sample. The grey bars indicate galaxies with no significant outflows, while red bars indicate galaxies with significant outflows.

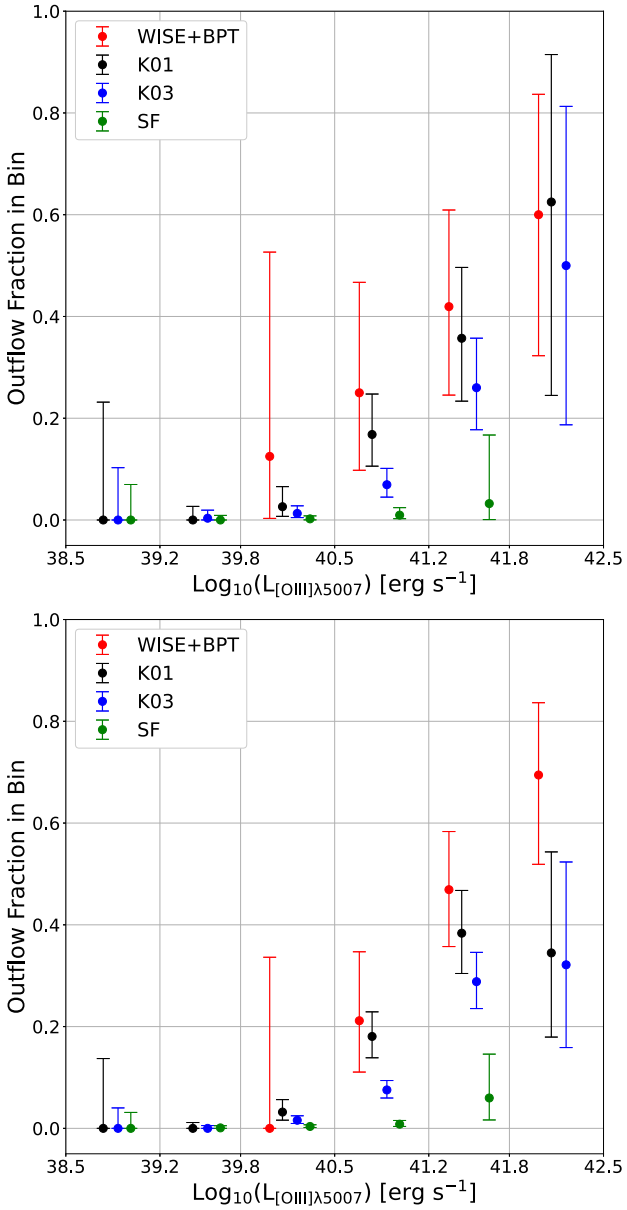

Figure 7. Outflow incidence as a function of [O III] λ5007 luminosity, separated into our various sub-samples for the entire merger (top panel) and control (bottom panel) sample. Errors are computed using binomial statistics with a two-sided 95 per cent confidence interval. Horizontal spacing between data points *within* each bin is arbitrary and only serves to enhance readability.

sub-classes, as can be seen in Fig. 7 where we plot the mean outflow fraction as a function of the [O III] λ5007 luminosity for each of the various sub-classes. It is readily apparent that while the outflow incidence increases with increasing [O III] λ5007 luminosity, the outflow fraction is consistently significantly higher in AGN compared with SF galaxies at all [O III] λ5007 luminosities. Further, optical + mid-infrared selected AGN display elevated outflow fractions compared with optically selected AGN, particularly at the highest [O III] λ5007 luminosities. Our results therefore indicate that the incidence of outflows is higher in AGNs, a result that is independent of total luminosity or SFR. Additionally, our findings suggest that mid-infrared selection in particular may favour outflows, a result that is reported for the first time in this work (see Sections 5.1 and 6 for further discussion of this result).

Finally, we also see from Table 1 that the SF galaxies typically have outflow velocities on the order of ∼300 km s^{-1} while AGNs typically have outflow velocities of the order of ∼700 km s^{-1}. This is again generally consistent with the literature (e.g. Rupke, Veilleux & Sanders 2002; Rupke et al. 2005b; Veilleux & Rupke 2005; Harrison et al. 2014; Liu et al. 2020; Smethurst et al. 2021). The average outflow velocity in our SF control sample is lower than the average AGN outflow velocity by about four sigma. We additionally note that there is no significant difference between the outflow velocity *among* our three AGN samples.

While there is a statistically significant enhancement in the [O III] λ5007 outflow luminosities in the AGN compared to the SF galaxies, this enhancement appears only marginal.

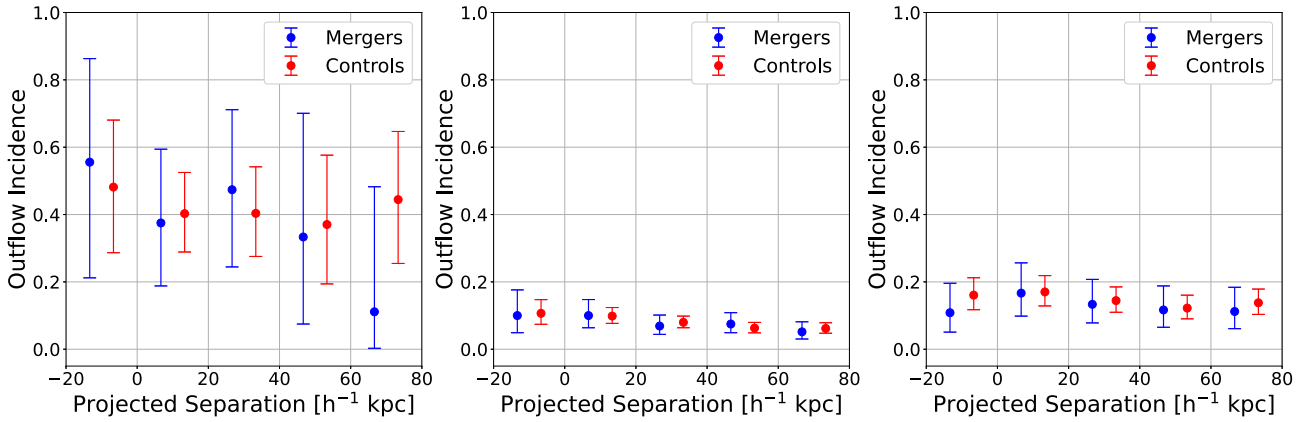

Figure 8. Average outflow incidence in each bin of projected physical separation r_p for the *WISE* + BPT sample (left-hand panel), K03 AGN (middle panel), and K01 AGN (right-hand panel). Errors are computed using binomial statistics with a 95 per cent confidence interval. Horizontal spacing between data points *within* each bin is arbitrary and only serves to enhance readability.

5 OUTFLOW CHARACTERISTICS AS A FUNCTION OF MERGER STAGE

In this section, we examine outflows as a function of merger stage.[3] In each plot, we bin the data in increments of 20 kpc. While this choice of binning is somewhat arbitrary, this particular choice allows for a generally acceptable number of objects in each bin, while still probing an acceptable range of r_p. Note that in all figures with r_p displayed on the horizontal axis, the first bin covering the −20 to 0 kpc range corresponds to the post-merger objects. As discussed in Section 2, our controls are matched in redshift, stellar mass, local density of galaxies, and [O III] λ5007 luminosity. SF galaxies are additionally matched in SFR.

5.1 Outflow incidence

Fig. 8 shows the average outflow incidence rate in each bin for both the mergers and controls as a function of r_p in AGN. As in Table 1, we compute error bars according to binomial statistics using a two-sided 95 per cent confidence interval – the confidence interval covers 2.5–97.5 per cent, or 95 per cent, of the uncertainty. Unlike in Table 1, we require all mergers to have three controls successfully analysed by BADASS in order to be included in this Figure. In Fig. 8, we see that the outflow fraction in the mergers and their matched controls shows no statistically significant difference in any r_p bin.

The *WISE* + BPT pairs and their controls typically have an outflow incidence around 40 per cent in each bin, with each bin typically having around 10 total mergers. While the post-mergers and their controls have an outflow incidence around 50 per cent, the large error bars in each bin suggest there is no significant difference between the merger and control samples in outflow incidence as r_p changes.

The outflow incidence in the optical AGN is much lower, with the K03 AGN incidence being slightly below 10 per cent in each bin and the K01 AGN being slightly above 10 per cent in each bin. The K03 AGN typically have a few hundred mergers in each bin, while the K01 AGN typically have around 100 mergers in each bin. In both cases, there is no statistically significant difference between the mergers and controls in each bin.

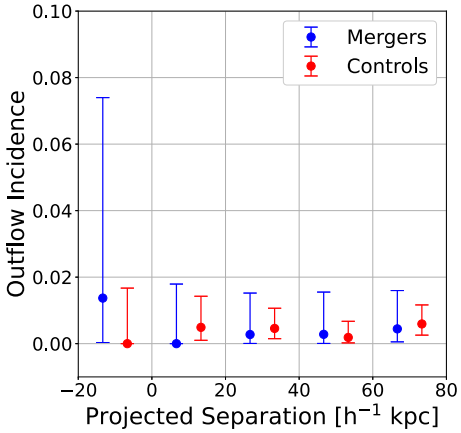

Figure 9. Average outflow incidence in each bin of projected physical separation r_p for K03 star-forming galaxies. Errors are computed using binomial statistics with a 95 per cent confidence interval. Horizontal spacing between data points *within* each bin is arbitrary and only serves to enhance readability.

Similarly, Fig. 9 shows the average outflow incidence in SF galaxies. The outflow incidence here is much less than the corresponding value for AGN, with a typical outflow incidence being only a fraction of a per cent. While there is an apparent jump in outflow incidence in the post-merger bin, this is because there are only 73 total objects in the post-merger bin (with a single outflow detection), while the other bins typically have a couple of hundred mergers in them.

Naively, it might be expected that the outflow incidence in both mergers and matched controls will increase at smaller pair separations, since AGN fraction and mid-infrared luminosity increase at smaller pair separations (Ellison et al. 2013a; Satyapal et al. 2014). However, this is not the case in our sample because of the way our sample is constructed. Since we require that mergers and controls are matched in [O III] λ5007 luminosity, the most luminous mergers, which are preferentially found at the smallest pair separations, do not have enough corresponding control galaxies with comparable luminosities and are therefore omitted from our sample. As a result, no enhancement in outflow incidence at smaller r_p is seen.

[3]Strictly speaking, we examine outflow properties as a function of the projected physical separation r_p. While later stage mergers are typically found at smaller values of r_p, paired galaxies can increase in r_p after a close encounter. Hence, it is possible to find a 'late stage' merger at higher r_p values.

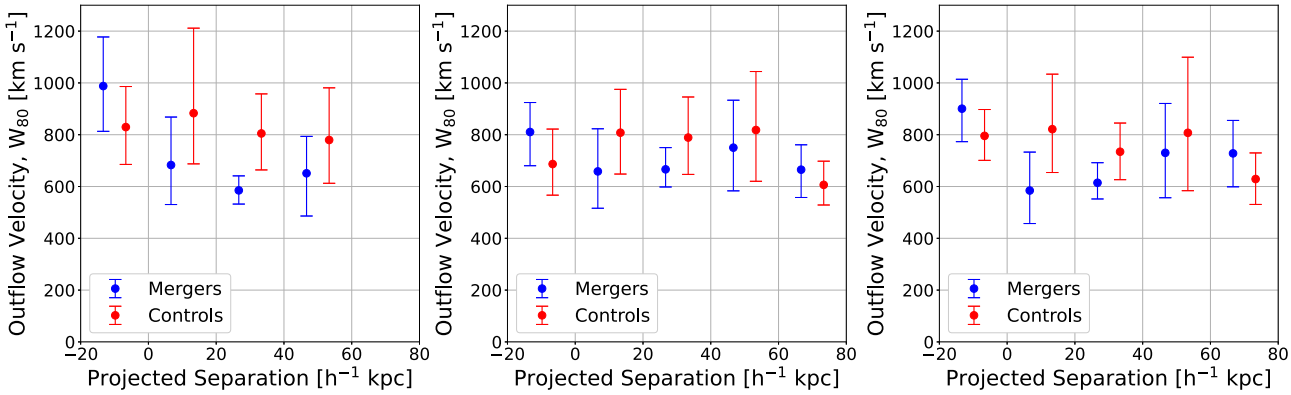

Figure 10. Average outflow velocity in each bin of projected physical separation r_p for the *WISE* + BPT sample (left-hand panel), K03 AGN sample (middle panel), and K01 AGN sample (right-hand panel). Errors are computed by averaging the upper (lower) uncertainties associated with each data point in each bin to obtain the final upper (lower) uncertainty for the average in each bin. Each merger is only required to have a minimum of *one* control with an outflow in order to be included in the plot. Horizontal spacing between data points *within* each bin is arbitrary and only serves to enhance readability.

Further, we note that the difference in the outflow occurrence rates between our samples is not *solely* due to different luminosity ranges between the samples. As discussed in Section 4, Fig. 7 shows that even for the same [O III] λ5007 luminosity range, SF galaxies have fewer outflows compared to AGN by a factor of about eight. Additionally, the K01 and K03 AGN samples have comparable luminosities across all r_p bins, yet outflows are more common in K01 AGN by as much as a factor of about two. While the *WISE* + BPT AGN do indeed have higher luminosities than the optical AGN in each r_p bin, we again see in Fig. 7 that even in the same luminosity bin, outflows are more common in the *WISE* + BPT sample by as much as a factor of about two at the highest [O III] λ5007 luminosities. This suggests that not only is the presence of an AGN necessary to create and drive powerful outflows, but the specific AGN selection technique can play an important role in characterizing the ionized outflows. We discuss the significance of the enhanced outflow rate in the *WISE* + BPT AGN in Section 6.

5.2 Outflow velocity

We also explore the outflow velocity in AGN mergers compared to their matched controls as a function of r_p. As discussed in Section 4, we use $W_{80} = 1.088$ FWHM to measure outflow velocity. However, we do not use the standard error of the mean to compute the uncertainties in this section. Each individual data point has its own upper and lower uncertainty value given by our final MCMC fit for each spectrum, and we attempt to take that uncertainty into account here. The uncertainties reported correspond to a 1σ level, so we multiply them by 1.96 for consistency with previous sections.[4] Fig. 10 shows the average outflow velocity for each r_p bin. The uncertainties on these data points are obtained by averaging the upper uncertainties together to obtain the average upper uncertainty, and similarly for the lower uncertainty.

In order for a velocity to be included in the plot, we must have a merger with an outflow and at least one control with an outflow. For this reason, the 60–80 kpc bin in the *WISE* + BPT outflow velocity plot does not contain any data points. The third bin (20–40 kpc) in this figure hints at a possible suppression of outflow velocities at this merger stage. However, this dearth is marginal and disappears if we use error bars corresponding to the 99 per cent level. The K03 and K01 AGN outflow velocities do not show any significant differences as a function of r_p. We do note that the *WISE* + BPT and K01 AGN outflow velocities are slightly elevated in the post-merger sample; however, the error bars in each of the bins are too large to draw any conclusions here. We omit the corresponding plot of the outflow velocity as a function of r_p for the SF sample because there are not enough outflows in this sample to make any meaningful remarks.

Fig. 11 shows the outflow velocities as a function of [O III] λ5007 luminosity for each sub-sample. First, we note that the SF sub-sample has systematically lower outflow velocities than the AGN samples at all luminosities. Further, as the [O III] λ5007 luminosity increases, the outflow velocity in the SF sub-sample steadily increases. However, we only observe a significant increase in outflow velocity in the highest luminosity bin for the AGN sub-samples. Evidently, the presence of an AGN is important in driving high-velocity outflows.

5.3 Outflow luminosity

Fig. 12 shows the outflow luminosity in the mergers and controls as a function of r_p for the three AGN sub-samples. Again, the final bin in the *WISE* + BPT AGN plot does not have any objects because there is no merger with an outflow that also has a control with an outflow in that bin. Since the uncertainty on the flux and redshift is exceedingly small for each object, we compute uncertainties using the standard error of the mean here. In all three sub-samples, we again see that there is no significant difference between the mergers and controls. Again, we omit the outflow luminosity figure for the SF sample because there are not enough outflows in this sample to draw any significant conclusions.

We note that since we have not matched our controls in SFR for AGN, it is important to examine the SFR in mergers and controls to see if this could impact possible outflow trends presented here. Fig. 13 shows the SFR as a function of r_p in the mergers and controls. For the *WISE* + BPT AGN sample we see that there is no appreciable difference between the merger and control SFR, though there is possible slight elevation seen in the post-merger bin and 60–80 kpc bin for the mergers. In the K01 and K03 AGN samples, we see a clear enhancement of the SFR in the post-mergers, and only the post-mergers. This is expected, since the SFR is known to naturally increase in our post-mergers sample (see figs 5 and 6 in Ellison

[4]The posterior distribution of the outflow FWHM parameter is generally Gaussian for objects that have an outflow.

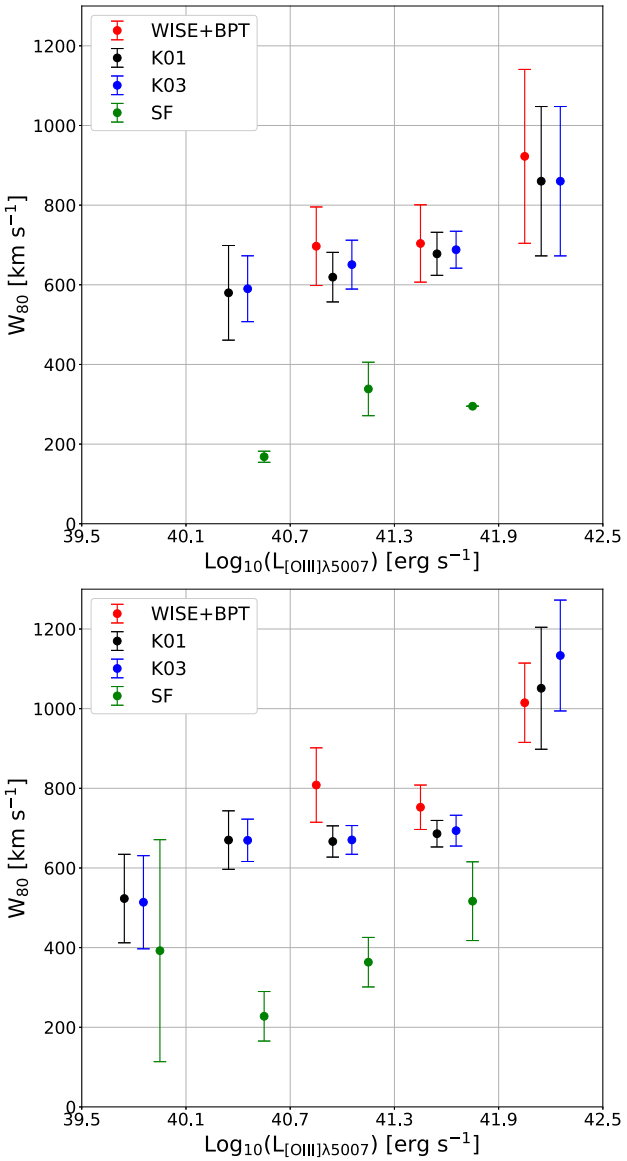

Figure 11. Average outflow velocity in each bin of [O III] λ5007 luminosity for the merger (top panel) and control (bottom panel), separated into our various sub-samples. Errors are computed using a 2σ standard error of the mean. Horizontal spacing between data points *within* each bin is arbitrary and only serves to enhance readability. The SF data point in the fourth bin of the merger plot has zero error because it is the only object in that bin.

et al. 2013b). However, elevations in SFR are unlikely to impact our results since the SFR enhancement in the post-merger bin is likely not sufficient to drive outflows as suggested by Fig. 7, where it is evident that the outflow incidence remains at zero per cent at all but the highest [O III] λ5007 luminosities. Hence, the effect of not matching our controls in SFR is insufficient to cause any significant impact on our results. Moreover, there is no enhancement in the outflow incidence, velocity, or luminosity in the post-merger bin that could be caused by an elevated SFR.

6 DISCUSSION

The above analysis yields several main results. First, we see in Figs 7 and 11 that the ionized outflow incidence and velocities, as traced by the [O III] λ5007 line, are significantly lower in SF galaxies compared with AGN even when normalizing by the luminosity of the [O III] λ5007 line. While the outflow incidence in both AGN and SF galaxies increases with the [O III] λ5007 luminosity, the outflow incidence is by far the greatest in galaxies that harbour an AGN. This general result is consistent with numerous other studies that report a low outflow incidence in SF galaxies compared to AGN (e.g. Cicone et al. 2014; Harrison et al. 2016; Concas et al. 2017; Leung et al. 2019; Lutz et al. 2020; Avery et al. 2021). Similarly, the outflow velocity in SF galaxies is significantly less than those galaxies hosting an AGN, ($\sim$300 km s^{-1} versus $\sim$700 km s^{-1}). We only note an increase in average outflow velocity in the most luminous [O III] λ5007 bins. While we do expect a correlation with outflow velocity and [O III] λ5007 luminosity, others (e.g. Veilleux et al. 2013; Fiore et al. 2017) have shown a much stronger trend with (bolometric) luminosity and outflow velocity. The discrepancy can, at least in part, be attributed to different measures of outflow velocity (e.g. using purely the velocity offset, 90th percentile of the emission line, or some combination of these) and different sample luminosity ranges (often being several orders of magnitude higher than ours). However, this may not *fully* explain our discrepancy with [O III] λ5007 luminosity and outflow velocity. Fig. 1 in Scholtz et al. (2021) shows a strong correlation between W_{80} and [O III] λ5007 luminosity for local ($z < 0.4$) AGN in *SDSS* in our luminosity range. While we do not find such a strong correlation, we note our results are self-consistent and are robust for the questions we are investigating.

It is important to note that outflow incidence rates vary widely throughout the literature. Our bulk outflow detection rates in our AGN sub-samples are slightly lower than the lower end estimates of outflow incidence found in the literature. For instance, Manzano-King et al. (2019), Roberts-Borsani et al. (2020), Wylezalek et al. (2020), Smethurst et al. (2021), and Avery et al. (2021) find outflow incidence rates in the $\sim$10–30 per cent range. However, Soto et al. (2012), Veilleux et al. (2013), Villar Martín et al. (2014), Perna et al. (2017), Toba et al. (2017), and Rakshit & Woo (2018) find that outflows are exceedingly common, at both moderate and high ($z \lesssim 2.6$) redshifts, with incidence rates in the $\sim$40–95 per cent range. There are many reasons for this wide range, including differences in spectral resolution (higher resolution data often find more outflows than lower resolution data), sample luminosities (outflows tend to be more common in galaxies with higher bolometric luminosities), and different fitting techniques. Even though outflow incidence is highly variable in the literature, overall trends such as outflow velocity/incidence increasing with bolometric luminosity, are generally consistent.

In SF galaxies, the outflow incidence shows a significant increase only at the highest [O III] λ5007 luminosities in our study, as indicated in Fig. 7. Indeed, the outflow incidence in SF galaxies is near zero per cent, except at the highest luminosities where it is about five per cent. Even then, the outflow detection rate is far below that found in the other sub-samples. This is consistent with other studies in which the outflow incidence is $\sim$zero per cent in galaxies at the lowest luminosities (e.g. Concas et al. 2017), but is significantly higher in more luminous SF galaxies at redshifts closer to the peak in the cosmic star formation history (e.g. Rubin et al. 2010, 2014; Kornei et al. 2012; Förster Schreiber et al. 2019), perhaps suggesting that there is some threshold above which SF can drive powerful outflows. Indeed, studies have suggested a minimum SFR surface density for outflows to be launched in SF galaxies at both moderate ($z \sim 1$) (Kornei et al. 2012) and low ($z \sim 0$) (Roberts-Borsani et al. 2020) redshifts. Again from Fig. 7, it is clear that for $\log_{10}(L_{[\mathrm{O\,III}]}$ [ergs s^{-1}]) $\gtrsim 40.5$ the outflow incidence for galaxies harbouring AGN is significantly above that for the SF galaxies with comparable

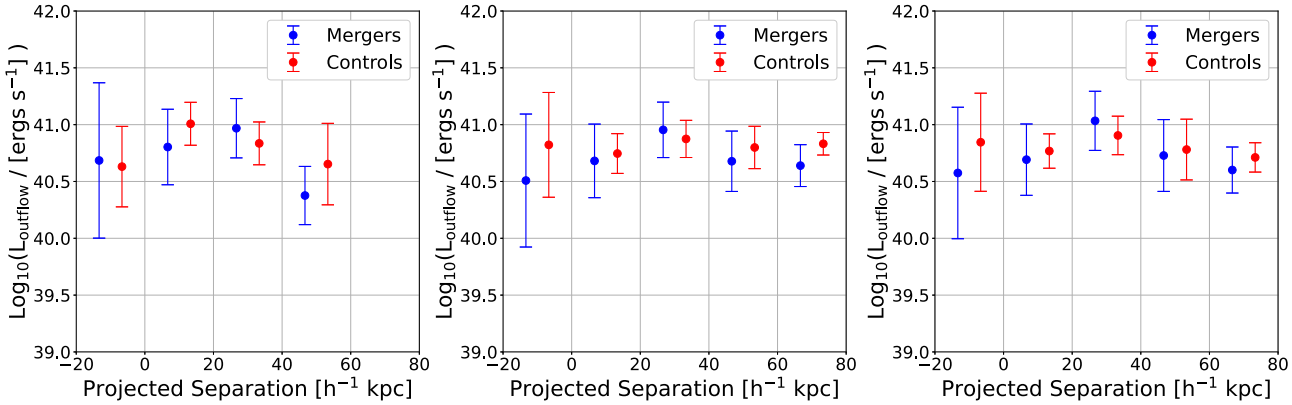

Figure 12. Average outflow Luminosity in each bin of projected physical separation r_p for the *WISE* + BPT sample (left-hand panel), K03 AGN sample (middle panel), and K01 AGN sample (right-hand panel). Errors are computed using a 2σ standard error of the mean. Each merger is only required to have a minimum of *one* control with an outflow in order to be included in the plot. Horizontal spacing between data points *within* each bin is arbitrary and only serves to enhance readability.

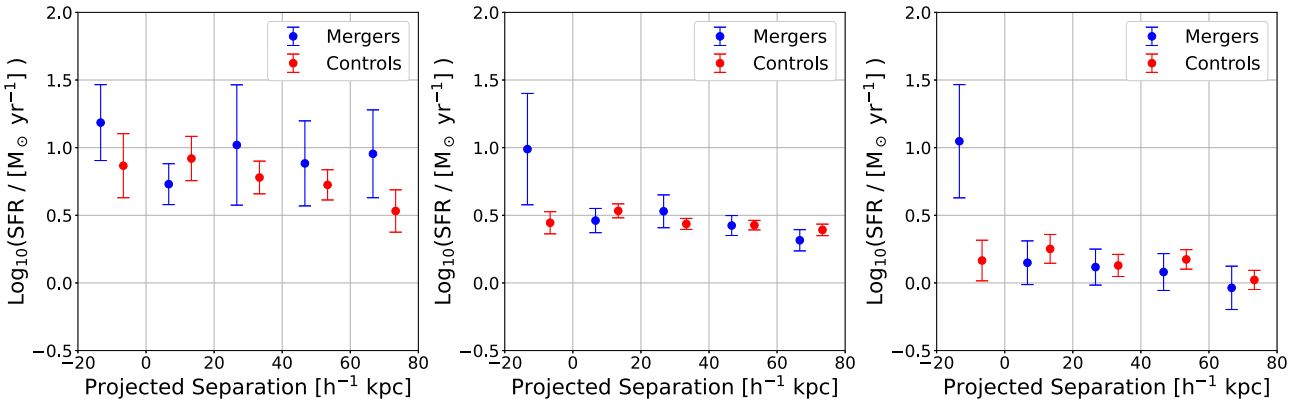

Figure 13. Average SFR in each bin of projected physical separation r_p for the *WISE* + BPT sample (left-hand panel), K03 AGN sample (middle panel), and K01 AGN sample (right-hand panel). Errors computed using a 2σ standard error of the mean. Horizontal spacing between data points *within* each bin is arbitrary and only serves to enhance readability.

luminosities – a result that is independent of presence or absence of a galaxy merger. This suggests that the presence and energetics of the AGN is needed to drive large-scale outflows, at least at these moderate luminosities. Alternatively, the conditions in the galaxies hosting AGNs could be such that it is easier to drive the outflow. For example, recent studies of the central kiloparsec region of AGN hosts have found lower molecular gas fractions compared with SF galaxies (Ellison et al. 2021), a result that is consistent with recent MaNGA IFU studies (Sánchez et al. 2018). The greatest molecular depletion factors found by Ellison et al. (2021) are at the highest luminosities, possibly suggesting that either the radiation field or shocks produced by the AGN reduces the central molecular gas fraction, making it easier to drive the currently observed outflows.

These results also suggest, for the first time, that the outflow incidence is dependent on the AGN selection technique, with Fig. 7 showing that optical + mid-infrared selected AGN have the highest outflow fraction compared to purely optical AGNs at a given luminosity, especially at the highest [O III] λ5007 luminosities. It is not immediately apparent why this might be the case. This result is not a consequence of differences in AGN luminosity between AGN classes, and the mid-infrared selected AGN in our sample are also required to be optically BPT AGNs. One possibility is that mid-infrared selected AGNs are found in galaxies with elevated star formation rates compared to optical AGN with the same luminosity, at least at higher luminosities. Hence, it is possible that both the AGN and enhanced star formation activity in these galaxies contribute to driving powerful outflows. Alternatively, the nuclear environment of our mid-infrared selected AGN may be denser than our optical AGN, thereby providing more raw material to power the outflow. It is worth noting that the outflow incidence in mid-infrared selected AGN is over 60 per cent at the highest luminosities, and may be slightly elevated compared to optical AGN in other higher luminosity bins. This 60 per cent outflow incidence is similar to Bohn et al. (2022), where they found ionized outflows in ∼60 per cent of their mid-infrared selected AGN, with similar [O III] λ5007 luminosities. Note, however, the outflow incidence in *WISE* + BPT AGN is only significantly elevated in the highest [O III] λ5007 luminosity bin in the control sample. While this result is only apparent in the control sample, the control sample has about two to three times the number of objects in each sample compared to the corresponding luminosity bin in the mergers (15 versus 36 *WISE* + BPT AGN, 8 versus 29 K01 AGN, and 10 versus 28 K03 AGN), hence our control sample provides a more statistically robust result. Further, while there is marginal overlap in the error bars at the 95 per cent confidence level, they do not overlap at the 93 per cent confidence level. To assess the true significance of the difference in outflow incidence between the *WISE* + BPT AGN and optical AGN in this bin, we utilize Fisher's exact test and a binomial Continuous Distribution Function (CDF)

to test for homogeneity between the samples. Our null hypothesis is that the *WISE* + BPT AGN and K01 AGN (or K03 AGN) have the same proportion of outflows. Fisher's exact test returns a p-value of only ∼0.003 in both sample comparisons. The binomial CDF returns a p-value of ∼0.03 in both sample comparisons. Therefore, we reject the null hypothesis and conclude that outflows are more common in the *WISE* + BPT AGN compared to optical AGN in the highest luminosity bin ($41.8 \leq L_{[\mathrm{O\,III}]\,\lambda5007} \leq 42.5$) to a confidence level greater than ∼97 per cent. Therefore, our work demonstrates that at the highest [O III] λ5007 luminosities, optical + mid-infrared selected AGNs do have a statistically significant higher outflow rate compared to AGNs that are only selected optically. Thus, at least at sufficiently high [O III] λ5007 luminosities, mid-infrared colour selection might be an effective strategy for finding outflows in large samples of galaxies.

The main result of this work is, while the galaxy sub-type and luminosity have a clear impact on the incidence and velocity of outflows, Figs 8 and 9 show that there is no statistically significant difference between these properties in mergers relative to a matched control sample, at any merger stage. We note that while the AGN incidence and SFR in mergers are generally expected to increase with decreasing pair separation, because we are requiring our controls to be matched in [O III] λ5007 luminosity, in addition to mass, redshift, and local galaxy density, we can isolate the role of the merging environment on the outflow properties. We note that the goal of this work is to determine the effect of the merger alone on the presence and properties of outflows. In order to perform the test we have designed, we must match in [O III] λ5007 luminosity when constructing our control sample because we know outflow incidence and velocity is correlated with luminosity. It is also clear that matching in stellar mass and redshift is critical since outflow incidence is found to be a function of stellar mass (e.g. Avery et al. 2021) and IFU studies have shown that outflows are centrally concentrated (Liu et al. 2020; Avery et al. 2021; Hogarth et al. 2021), indicating that aperture size will strongly impact outflow detection and properties. After these matching criteria are met, it is clear that there is no effect on the presence, velocity, and luminosity of outflows that results from the merger environment, at least as traced by the [O III] λ5007 line.

If galaxy mergers cause gas inflows induced by gravitational torques, one might suppose that the outflows might be more difficult to drive in galaxy mergers compared to their matched controls. However our study demonstrates that no such impact is seen in the large-scale outflows. We note that in this work, we only explore the presence of ionized outflows, their velocities, and their luminosities. The derived outflow properties, such as the mass outflow rate and mass loading factor, require knowledge of additional parameters such as the radial extent of the outflow and the electron density in the outflowing gas, which are difficult or impossible to constrain given the single aperture data presented here. As discussed in Harrison et al. (2018), the electron density alone is a large source of uncertainty in these energetics calculations, with resulting calculations having up to three orders of magnitude uncertainty. We are also limited to the spatial regions covered by the *SDSS* fibres, so we cannot explore the spatial extent of the outflows. A robust determination of the outflow energetics will require high signal-to-noise and high spatial resolution IFU data in order to constrain the extent and mass of the outflow. Thus, while there is no clear difference in the outflow incidence and velocities in mergers relative to isolated controls, the mass outflow rates could be different, particularly if there are differences in the electron density within the entrained wind or in the spatial extent of the warm ionized gas in mergers relative to their matched controls.

While there have not been any large-scale systematic studies that compare outflow properties in various merger stages relative to a robust control sample, Hill & Zakamska (2014) examined 115 ULIRGs for excess H_2 emission, which they interpreted as evidence of an outflow. Their findings are mixed. They find a weak positive correlation between H_2 and tidal tails of a galaxy, whose length can be used to estimate the stage of a galaxy merger. This correlation suggests that the outflows they found are more likely to be in advanced mergers. However, they do not find evidence of H_2 being correlated with nuclear separation. It should be stressed that, unlike this work, their study did not compare their mergers to a robust control sample. None the less, their findings also suggest that there is no correlation between outflows and mergers, and no dependence on merger stage.

It is important to note several caveats to our work. First, we do not explicitly match our AGN sub-sample in SFR. As a result, the SFR in our post-merger sample is enhanced relative to their controls. However, this enhancement in SFR does not produce an excess of outflows in our post-merger sample, implying that the SFR is not high enough to influence the results of our study. Secondly, the ionized outflows probed by the [O III] λ5007 line are based on single-fibre observations. There could be differences in mergers relative to their controls seen in the centrally concentrated gas – the outflow signatures could be diluted in the larger aperture observations presented here. Indeed, Debuhr et al. (2010) suggest that major mergers can enhance outflows in the nuclear region of galaxies, but cannot generate large-scale outflows. Higher spatial resolution observations would be required to explore differences on scales closer to those at which the outflows are physically launched. The *SDSS* utilizes a three arcsec fibre, which corresponds to a physical distance of ∼5 ± 2 kpc at a redshift of 0.0835 ± 0.0355 (the average and standard deviation of the redshift in our pair sample), which is comparable to the effective radius of the galaxies in our sample. While aperture effects may play a role, recent MaNGA results (e.g. Avery et al. 2021) have shown that the outflows traced by the [O III] λ5007 line are centrally concentrated, with ∼67 per cent of outflowing galaxies showing the bulk of their broad-component wind signature encompassed within the effective radius of the galaxy. Further, there could be systematic differences in the attenuation of the optical emission lines in mergers relative to the controls, either as a result of foreground material from the inflowing gas from the merger, or changes in the dust attenuation in the entrained wind as a result of metallicity changes in the outflowing gas from the merger. There could also be differences in the metal enrichment of the outflowing gas from nuclear star formation, a phenomenon that has been previously suggested in low-redshift galaxies in the MaNGA survey by Avery et al. (2021). Further, it is possible that the inflowing gas in mergers could cause significant obscuration of the optical line emission, preferentially causing outflows in mergers to be more elusive than in the control when using optical lines. We examine this possibility by plotting the extinction, as measured by $E(B-V)$, as a function of r_p. Fig. 14 shows the extinction in mergers and controls in each bin for our AGN sub-samples. Note that in the *WISE* + BPT AGN extinction we see an elevated extinction in the post-mergers for *both* the mergers and controls. In the K03 and K01 AGN, we see that there is a significantly heightened extinction in the mergers compared to the controls in nearly every r_p bin. Fig. 15 shows a similar extinction plot for SF galaxies. In any case, we see that there is generally a higher level of obscuration in the mergers compared to the controls in all sub-samples, except in the *WISE* + BPT sample. Finally, we note that the [O III] λ5007 luminosity may not be reliable for tracing AGN luminosity in the *WISE* + BPT AGN

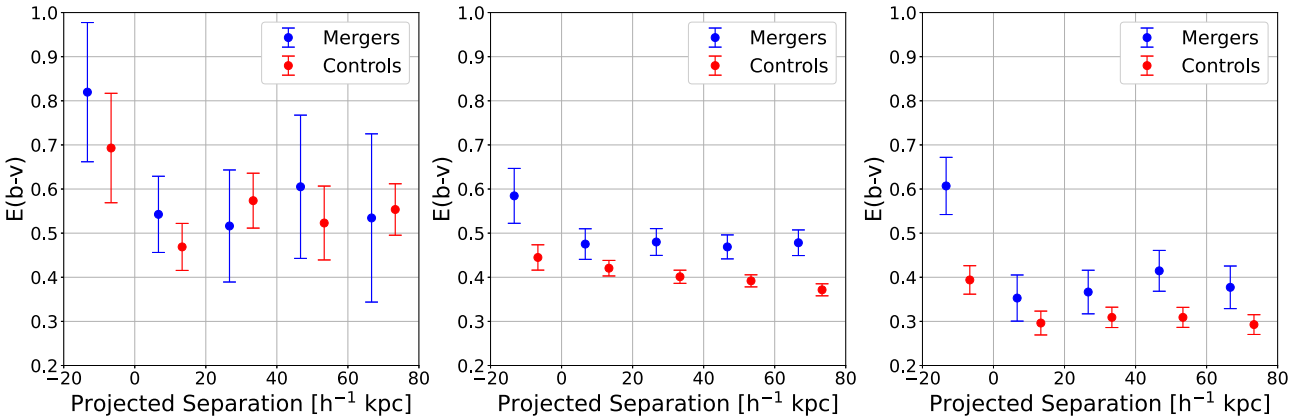

Figure 14. Average dust extinction in each bin of projected physical separation r_p for the *WISE* + BPT sample (left-hand panel), K03 AGN sample (middle panel), and K01 AGN sample (right-hand panel). Errors are computed using a 2σ standard error of the mean. Horizontal spacing between data points *within* each bin is arbitrary and only serves to enhance readability.

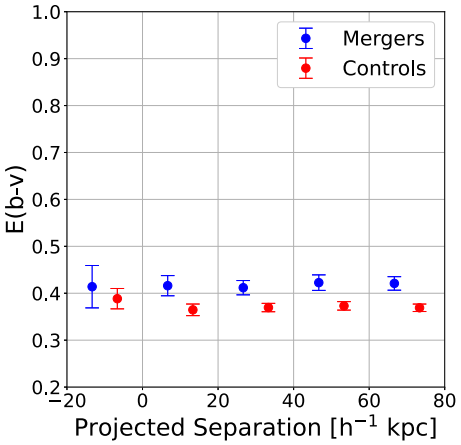

Figure 15. Average extinction in each bin of projected physical separation r_p for SF galaxies. Errors computed using a 2σ standard error of the mean. Horizontal spacing between data points *within* each bin is arbitrary and only serves to enhance readability.

sample. As shown in Fig. 14, the *WISE* + BPT AGN tend to be more heavily obscured than the optical AGN. If the central AGN in the *WISE* + BPT sample additionally heats the dust near the central engine, the [O III] λ5007 line might not be as accurate of a tracer for AGN bolometric luminosity as it is in the less obscured optically identified AGN.

7 CONCLUSIONS

In this paper, we have conducted the first large-scale systematic study of ionized outflows in galaxy pairs and post-mergers matched to a carefully constructed, robust control sample in order to determine the effect of mergers on the prevalence and properties of these outflows, and to explore the dependence on merger stage. Our sample consists of ∼4000 galaxies at various merger stages drawn from the *SDSS DR7*, comprised of SF galaxies, optical AGN, and mid-infrared colour-selected AGN, classified based on the K01 and K03 AGN classification schemes. Each merger is matched in stellar mass, redshift, local density of galaxies and [O III] λ5007 luminosity (SF galaxies are additionally matched in SFR) to three isolated control galaxies. We examined the kinematics of the [O III] λ5007 emission line to search for blueshifted, asymmetrical emission line profiles, which are interpreted as ionized outflows. Our results are summarized as follows:

(i) The merging environment has no statistically significant impact on the incidence or properties of the ionized outflows, and there is no dependence seen on merger stage.

(ii) Ionized outflows are significantly less common in SF galaxies compared to galaxies that host an AGN in the sample as a whole, even when normalizing by the luminosity of the [O III] λ5007 line. This result is consistent with numerous other studies exploring ionized outflows in galaxies. Further, outflows are much less common in LINERs compared to Seyferts.

(iii) The outflow incidence and velocity increase with [O III] λ5007 luminosity for both SF galaxies and galaxies harbouring AGN. In contrast to AGN, there is a threshold in the SF galaxies of $\log_{10}(L_{[\mathrm{O\,III}]}\ (\mathrm{ergs\ s^{-1}})) \gtrsim 41.5$ below which the outflow incidence is near zero per cent.

(iv) Outflow velocities are lowest in the SF galaxies, with an average of ∼300 km s^{-1}. The average outflow velocity in all AGN sub-samples is ∼700 km s^{-1}.

(v) The outflow incidence depends on the presence of AGN and AGN selection technique, with optical+mid-infrared selected AGN showing the largest outflow incidence. SF galaxies have an outflow incidence of only ∼0.5 per cent, while K03 AGN have an incidence of ∼7 per cent and K01 AGN have an incidence of ∼14 per cent. Optical + mid-infrared selected AGN have an average incidence of ∼40 per cent, with an incidence rate of ∼60 per cent at the highest [O III] λ5007 luminosities. Mid-infrared colour selection may therefore be an effective pre-selection strategy for finding outflows in large samples of galaxies.

(vi) The outflow luminosity is lowest in SF galaxies, with an average of $\log_{10}(L_{\mathrm{outflow}}[\mathrm{ergs\ s^{-1}}])$ ∼40.0. AGNs have a slightly elevated average outflow luminosity of $\log_{10}(L_{\mathrm{outflow}}[\mathrm{ergs\ s^{-1}}])$ ∼40.7.

While these results suggest that the merging environment does not have a significant impact on the presence or properties of ionized outflows, our observations are based on large aperture, single-fibre observations. If outflows are more concentrated in the centres of galaxies, the signatures of the outflowing gas could be diluted in the spectra analysed here. Further, optical emission lines in mergers could be more heavily attenuated compared to the controls. Near-infrared spectroscopic observations are necessary to fully understand

the effects of extinction and the resulting impact on the outflow incidence and properties. In order to obtain a complete understanding of how ionized outflows behave in mergers, higher spatial resolution near-infrared IFU data are needed.

ACKNOWLEDGEMENTS

The authors thank the anonymous referee for providing insightful feedback that improved the quality and clarity of the manuscript. WM is grateful to R. Weigel for discussions on the statistical analysis conducted in this work, T. Bohn for his helpful plotting routines, and S. Silayi for advice on fitting spectra efficiently. GC acknowledges support by the National Science Foundation, under grant No. AST 1817233. LB acknowledges support from National Aeronautics and Space Administration award #80NSSC20K0502. This publication makes use of data products from the *Wide-field Infrared Survey Explorer*, which is a joint project of the University of California, Los Angeles, and the Jet Propulsion Laboratory/California Institute of Technology, funded by the National Aeronautics and Space Administration. We are grateful to the MPA/JHU group for access to their data products and catalogues (maintained by Jarle Brinchmann at http://www.mpa-garching.mpg.de/SDSS/). Funding for the SDSS and SDSS–II has been provided by the Alfred P. Sloan Foundation, the Participating Institutions, the National Science Foundation, the U.S. Department of Energy, the National Aeronautics and Space Administration, the Japanese Monbukagakusho, the Max Planck Society, and the Higher Education Funding Council for England. The SDSS Web Site is http://www.sdss.org/. The SDSS is managed by the Astrophysical Research Consortium for the Participating Institutions. The Participating Institutions are the American Museum of Natural History, Astrophysical Institute Potsdam, University of Basel, University of Cambridge, Case Western Reserve University, University of Chicago, Drexel University, Fermilab, the Institute for Advanced Study, the Japan Participation Group, Johns Hopkins University, the Joint Institute for Nuclear Astrophysics, the Kavli Institute for Particle Astrophysics and Cosmology, the Korean Scientist Group, and the Chinese Academy.

The spectral fits carried out in this work were run on ARGO, a research computing cluster provided by the Office of Research Computing at George Mason University, VA. (http://orc.gmu.edu). This research made use of Astropy,[5] a community-developed core Python package for Astronomy (Astropy Collaboration et al. 2018), as well as TOPCAT (Taylor 2005).

DATA AVAILABILITY

The data sets used in this publication were derived from the open-source code Bayesian AGN Decomposition Analysis for *SDSS* Spectra available at https://github.com/remingtonsexton/BADASS3, the *Wide-field Infrared Survey Explorer* (https://wise2.ipac.caltech.edu/docs/release/allsky/), the MPA/JHU catalogue (http://www.mpa-garching.mpg.de/SDSS/), and the *Sloan Digital Sky Survey* (*SDSS*; http://www.sdss.org/). Our sample was assembled from the *SDSS* Data Release 7 Main Galaxy Sample (Abazajian et al. 2009). Corresponding spectra were queried from the SDSS Data Release 12 (Alam et al. 2015), which can be accessed from the traditional Science Archive Server https://dr12.sdss.org/sas. The processed data sets underlying this article will be shared on reasonable request to the corresponding author.

[5]http://www.astropy.org

REFERENCES

Abazajian K. N. et al., 2009, ApJS, 182, 543
Agostino C. J. et al., 2021, ApJ, 922, 156
Alam S. et al., 2015, ApJS, 219, 12
Astropy Collaboration et al., 2018, AJ, 156, 123
Avery C. R. et al., 2021, MNRAS, 503, 5134
Bae H.-J., Woo J.-H., 2016, ApJ, 828, 97
Baldwin J. A., Phillips M. M., Terlevich R., 1981, PASP, 93, 5
Balmaverde B. et al., 2016, A&A, 585, A148
Barnes J. E., Hernquist L. E., 1991, ApJ, 370, L65
Baron D. et al., 2018, MNRAS, 480, 3993
Barrows R. S., Sandberg Lacy C. H., Kennefick J., Comerford J. M., Kennefick D., Berrier J. C., 2013, ApJ, 769, 95
Blecha L., Snyder G. F., Satyapal S., Ellison S. L., 2018, MNRAS, 478, 3056
Blumenthal K. A., Barnes J. E., 2018, MNRAS, 479, 3952
Bohn T., Canalizo G., Satyapal S., Sales L. V., 2022, ApJ, 931, 69
Brinchmann J., Charlot S., White S. D. M., Tremonti C., Kauffmann G., Heckman T., Brinkmann J., 2004, MNRAS, 351, 1151
Bruce V. A., Dunlop J. S., Mortlock A., Kocevski D. D., McGrath E. J., Rosario D. J., 2016, MNRAS, 458, 2391
Canalizo G., Stockton A., 2001, ApJ, 555, 719
Carniani S. et al., 2015, A&A, 580, A102
Cicone C. et al., 2014, A&A, 562, A21
Cicone C., Maiolino R., Marconi A., 2016, A&A, 588, A41
Cisternas M. et al., 2011, ApJ, 726, 57
Comerford J. M., Nevin R., Stemo A., Müller-Sánchez F., Barrows R. S., Cooper M. C., Newman J. A., 2018, ApJ, 867, 66
Concas A., Popesso P., Brusa M., Mainieri V., Erfanianfar G., Morselli L., 2017, A&A, 606, A36
Cresci G. et al., 2015, A&A, 582, A63
Darg D. W. et al., 2010, MNRAS, 401, 1043
Davies R. L. et al., 2019, ApJ, 873, 122
Debuhr J., Quataert E., Ma C.-P., Hopkins P., 2010, MNRAS, 406, L55
Ellison S. L., Patton D. R., Simard L., McConnachie A. W., 2008, AJ, 135, 1877
Ellison S. L., Patton D. R., Simard L., McConnachie A. W., Baldry I. K., Mendel J. T., 2010, MNRAS, 407, 1514
Ellison S. L., Patton D. R., Mendel J. T., Scudder J. M., 2011, MNRAS, 418, 2043
Ellison S. L., Mendel J. T., Scudder J. M., Patton D. R., Palmer M. J. D., 2013a, MNRAS, 430, 3128
Ellison S. L., Mendel J. T., Patton D. R., Scudder J. M., 2013b, MNRAS, 435, 3627
Ellison S. L., Patton D. R., Hickox R. C., 2015, MNRAS, 451, L35
Ellison S. L., Viswanathan A., Patton D. R., Bottrell C., McConnachie A. W., Gwyn S., Cuillandre J.-C., 2019, MNRAS, 487, 2491
Ellison S. L. et al., 2021, MNRAS, 505, L46
Fensch J. et al., 2017, MNRAS, 465, 1934
Fiore F. et al., 2017, A&A, 601, A143
Fluetsch A. et al., 2019, MNRAS, 483, 4586
Fluetsch A. et al., 2021, MNRAS, 505, 5753
Foreman-Mackey D., Hogg D. W., Lang D., Goodman J., 2013, PASP, 125, 306
Förster Schreiber N. M. et al., 2019, ApJ, 875, 21
Geach J. E. et al., 2018, ApJ, 864, L1
Gehrels N., 1986, ApJ, 303, 336
Genzel R. et al., 2011, ApJ, 733, 101
Goulding A. D. et al., 2018, PASJ, 70, S37
Guolo-Pereira M., Ruschel-Dutra D., Storchi-Bergmann T., Schnorr-Müller A., Cid Fernandes R., Couto G., Dametto N., Hernandez-Jimenez J. A., 2021, MNRAS, 502, 3618
Harrison C. M., Alexander D. M., Mullaney J. R., Swinbank A. M., 2014, MNRAS, 441, 3306
Harrison C. M. et al., 2016, MNRAS, 456, 1195
Harrison C. M., Costa T., Tadhunter C. N., Flütsch A., Kakkad D., Perna M., Vietri G., 2018, Nat. Astron., 2, 198
Heckman T. M., Armus L., Miley G. K., 1990, ApJS, 74, 833

Hermosa Muñoz L., Márquez I., Cazzoli S., Masegosa J., Agís-González B., 2022, A&A, 660, A133
Herrera-Camus R. et al., 2020, A&A, 635, A47
Hill M. J., Zakamska N. L., 2014, MNRAS, 439, 2701
Hogarth L. M. et al., 2021, MNRAS, 500, 3802
Holt J., Tadhunter C. N., Morganti R., 2008, MNRAS, 387, 639
Hopkins P. F., Hernquist L., Cox T. J., Di Matteo T., Robertson B., Springel V., 2006, ApJS, 163, 1
Hopkins P. F., Cox T. J., Kereš D., Hernquist L., 2008, ApJS, 175, 390
Kakkad D. et al., 2016, A&A, 592, A148
Kauffmann G. et al., 2003, MNRAS, 346, 1055
Kaviraj S. et al., 2013, MNRAS, 429, L40
Kewley L. J., Heisler C. A., Dopita M. A., Lumsden S., 2001, ApJS, 132, 37
Kewley L. J., Rupke D., Zahid H. J., Geller M. J., Barton E. J., 2010, ApJ, 721, L48
Khochfar S., Silk J., 2011, MNRAS, 410, L42
Kocevski D. D. et al., 2012, ApJ, 744, 148
Kornei K. A., Shapley A. E., Martin C. L., Coil A. L., Lotz J. M., Schiminovich D., Bundy K., Noeske K. G., 2012, ApJ, 758, 135
Lackner C. N. et al., 2014, AJ, 148, 137
Leung G. C. K. et al., 2019, ApJ, 886, 11
Lintott C. J. et al., 2008, MNRAS, 389, 1179
Liu X., Shen Y., Strauss M. A., 2012, ApJ, 745, 94
Liu W., Veilleux S., Canalizo G., Rupke D. S. N., Manzano-King C. M., Bohn T. U V., 2020, ApJ, 905, 166
Lutz D. et al., 2020, A&A, 633, A134
Manzano-King C. M., Canalizo G., Sales L. V., 2019, ApJ, 884, 54
Mechtley M. et al., 2016, ApJ, 830, 156
Mendel J. T., Simard L., Palmer M., Ellison S. L., Patton D. R., 2014, ApJS, 210, 3
Molyneux S. J., Harrison C. M., Jarvis M. E., 2019, A&A, 631, A132
Mullaney J. R., Alexander D. M., Fine S., Goulding A. D., Harrison C. M., Hickox R. C., 2013, MNRAS, 433, 622
Müller-Sánchez F., Comerford J. M., Nevin R., Barrows R. S., Cooper M. C., Greene J. E., 2015, ApJ, 813, 103
Nestor D. B., Johnson B. D., Wild V., Ménard B., Turnshek D. A., Rao S., Pettini M., 2011, MNRAS, 412, 1559
Nevin R., Comerford J. M., Müller-Sánchez F., Barrows R., Cooper M. C., 2018, MNRAS, 473, 2160
Patton D. R., Ellison S. L., Simard L., McConnachie A. W., Mendel J. T., 2011, MNRAS, 412, 591
Patton D. R., Torrey P., Ellison S. L., Mendel J. T., Scudder J. M., 2013, MNRAS, 433, L59
Patton D. R., Qamar F. D., Ellison S. L., Bluck A. F. L., Simard L., Mendel J. T., Moreno J., Torrey P., 2016, MNRAS, 461, 2589
Pearson W. J. et al., 2019, A&A, 631, A51
Pereira-Santaella M. et al., 2018, A&A, 616, A171
Perez J., Tissera P., Blaizot J., 2009, MNRAS, 397, 748
Perna M., Lanzuisi G., Brusa M., Mignoli M., Cresci G., 2017, A&A, 603, A99
Perret V., Renaud F., Epinat B., Amram P., Bournaud F., Contini T., Teyssier R., Lambert J.-C., 2014, A&A, 562, A1
Rakshit S., Woo J.-H., 2018, ApJ, 865, 5
Roberts-Borsani G. W., Saintonge A., Masters K. L., Stark D. V., 2020, MNRAS, 493, 3081
Rosario D. J., McGurk R. C., Max C. E., Shields G. A., Smith K. L., Ammons S. M., 2011, ApJ, 739, 44
Rosario D. J. et al., 2015, A&A, 573, A85
Rothberg B., Joseph R. D., 2004, AJ, 128, 2098
Rubin K. H. R., Weiner B. J., Koo D. C., Martin C. L., Prochaska J. X., Coil A. L., Newman J. A., 2010, ApJ, 719, 1503
Rubin K. H. R., Prochaska J. X., Koo D. C., Phillips A. C., Martin C. L., Winstrom L. O., 2014, ApJ, 794, 156
Rupke D., 2018, Galaxies, 6, 138
Rupke D. S., Veilleux S., Sanders D. B., 2002, ApJ, 570, 588
Rupke D. S., Veilleux S., Sanders D. B., 2005a, ApJS, 160, 87
Rupke D. S., Veilleux S., Sanders D. B., 2005b, ApJS, 160, 115
Rupke D. S., Veilleux S., Sanders D. B., 2005c, ApJ, 632, 751
Rupke D. S. N., Gültekin K., Veilleux S., 2017, ApJ, 850, 40
Sánchez S. F. et al., 2018, Rev. Mex. Astron. Astrofis., 54, 217
Santoro F., Tadhunter C., Baron D., Morganti R., Holt J., 2020, A&A, 644, A54
Satyapal S., Ellison S. L., McAlpine W., Hickox R. C., Patton D. R., Mendel J. T., 2014, MNRAS, 441, 1297
Schawinski K., Koss M., Berney S., Sartori L. F., 2015, MNRAS, 451, 2517
Scholtz J. et al., 2021, MNRAS, 505, 5469
Schweizer F., 1982, ApJ, 252, 455
Scudder J. M., Ellison S. L., Mendel J. T., 2012a, MNRAS, 423, 2690
Scudder J. M., Ellison S. L., Torrey P., Patton D. R., Mendel J. T., 2012b, MNRAS, 426, 549
Scudder J. M., Ellison S. L., Momjian E., Rosenberg J. L., Torrey P., Patton D. R., Fertig D., Mendel J. T., 2015, MNRAS, 449, 3719
Sexton R. O., Matzko W., Darden N., Canalizo G., Gorjian V., 2021, MNRAS, 500, 2871
Shah E. A. et al., 2020, ApJ, 904, 107
Shen Y., Liu X., Greene J. E., Strauss M. A., 2011, ApJ, 735, 48
Silk J., 2013, ApJ, 772, 112
Simmons B. D., Urry C. M., Schawinski K., Cardamone C., Glikman E., 2012, ApJ, 761, 75
Smethurst R. J., Simmons B. D., Lintott C. J., Shanahan J., 2019, MNRAS, 489, 4016
Smethurst R. J. et al., 2021, MNRAS, 507, 3985
Soto K. T., Martin C. L., 2012, ApJS, 203, 3
Soto K. T., Martin C. L., Prescott M. K. M., Armus L., 2012, ApJ, 757, 86
Springel V., Di Matteo T., Hernquist L., 2005, MNRAS, 361, 776
Stasińska G., Cid Fernandes R., Mateus A., Sodré L., Asari N. V., 2006, MNRAS, 371, 972
Sturm E. et al., 2011, ApJ, 733, L16
Swinbank A. M. et al., 2019, MNRAS, 487, 381
Taylor M. B., 2005, in Shopbell P., Britton M., Ebert R., eds, ASP Conf. Ser. Vol. 347, Astronomical Data Analysis Software and Systems XIV. Astron. Soc. Pac., San Francisco, p. 29
Thorp M. D., Ellison S. L., Simard L., Sánchez S. F., Antonio B., 2019, MNRAS, 482, L55
Toba Y., Bae H.-J., Nagao T., Woo J.-H., Wang W.-H., Wagner A. Y., Sun A.-L., Chang Y.-Y., 2017, ApJ, 850, 140
Toomre A., Toomre J., 1972, ApJ, 178, 623
Veilleux S., Rupke D. S., 2005, in Braun R., ed., ASP Conf. Ser. Vol. 331, Extra-Planar Gas. Astron. Soc. Pac., San Francisco, p. 313
Veilleux S. et al., 2013, ApJ, 776, 27
Veilleux S., Maiolino R., Bolatto A. D., Aalto S., 2020, A&AR, 28, 2
Villar Martín M., Emonts B., Humphrey A., Cabrera Lavers A., Binette L., 2014, MNRAS, 440, 3202
Villforth C. et al., 2014, MNRAS, 439, 3342
Villforth C. et al., 2017, MNRAS, 466, 812
Weiner B. J. et al., 2009, ApJ, 692, 187
Westmoquette M. S., Clements D. L., Bendo G. J., Khan S. A., 2012, MNRAS, 424, 416
Weston M. E., McIntosh D. H., Brodwin M., Mann J., Cooper A., McConnell A., Nielsen J. L., 2017, MNRAS, 464, 3882
Wong K. C. et al., 2011, ApJ, 728, 119
Woods D. F., Geller M. J., Kurtz M. J., Westra E., Fabricant D. G., Dell'Antonio I., 2010, AJ, 139, 1857
Woo J.-H., Bae H.-J., Son D., Karouzos M., 2016, ApJ, 817, 108
Wylezalek D., Flores A. M., Zakamska N. L., Greene J. E., Riffel R. A., 2020, MNRAS, 492, 4680
Xu C. K. et al., 2012, ApJ, 760, 72
Zakamska N. L., Greene J. E., 2014, MNRAS, 442, 784
Zakamska N. L. et al., 2016, MNRAS, 459, 3144
Zubovas K., Nayakshin S., King A., Wilkinson M., 2013, MNRAS, 433, 3079

This paper has been typeset from a TEX/LATEX file prepared by the author.